AGU PUBLICATIONS

JGR

Journal of Geophysical Research: Atmospheres

RESEARCH ARTICLE

10.1002/2016JD025906

Key Points:
- P-QCLAS is demonstrated to be a well-suited technique for high-precision, long-term, online monitoring of N_2O stable isotopic composition
- N_2O sources were isotopically lighter than tropospheric background air but showed unexpectedly high variability
- $\delta^{18}O$ may be a useful tracer for discerning urban/industry versus agricultural N_2O sources

Supporting Information:
- Supporting Information S1

Correspondence to:
E. Harris,
eliza.harris@uibk.ac.at

Citation:
Harris, E., S. Henne, C. Hüglin, C. Zellweger, B. Tuzson, E. Ibraim, L. Emmenegger, and J. Mohn (2017), Tracking nitrous oxide emission processes at a suburban site with semicontinuous, in situ measurements of isotopic composition, *J. Geophys. Res. Atmospheres*, *122*, 1850–1870, doi:10.1002/2016JD025906.

Received 6 SEP 2016
Accepted 19 DEC 2016
Accepted article online 13 JAN 2017
Published online 2 FEB 2017

Tracking nitrous oxide emission processes at a suburban site with semicontinuous, in situ measurements of isotopic composition

Eliza Harris[1,2], Stephan Henne[1], Christoph Hüglin[1], Christoph Zellweger[1], Béla Tuzson[1], Erkan Ibraim[1], Lukas Emmenegger[1], and Joachim Mohn[1]

[1]Laboratory for Air Pollution and Environmental Technology, Empa, Dübendorf, Switzerland, [2]Now at Plant, Soil and Ecosystem Processes Research Group, Institute of Ecology, University of Innsbruck, Innsbruck, Austria

Abstract The isotopic composition of atmospheric nitrous oxide (N_2O) was measured semicontinuously, at ~35 min frequency in intermittent periods of 1–6 days over one and a half years, using preconcentration coupled to a quantum cascade laser spectrometer at the suburban site of Dübendorf, Switzerland. The achieved measurement repeatability was 0.08‰, 0.11‰, and 0.10‰ for $\delta^{18}O$, site preference, and $\delta^{15}N^{bulk}$ respectively, which is better than or equal to standard flask sampling-based isotope ratio mass spectrometry performance. The observed mean diurnal cycle reflected the buildup of N_2O from isotopically light sources on an isotopically heavy tropospheric background. The measurements were used to determine the source isotopic composition, which varied significantly compared to chemical and meteorological parameters monitored at the site. FLEXPART-COSMO transport modeling in combination with modified Emissions Database for Global Atmospheric Research inventory emissions was used to model N_2O mole fractions at the site. Additionally, isotopic signatures were estimated for different source categories using literature data and used to simulate N_2O isotopic composition over the measurement period. The model was able to capture variability in N_2O mole fraction well, but simulations of isotopic composition showed little agreement with observations. In particular, measured source isotopic composition exhibited one magnitude larger variability than simulated, clearly indicating that the range of isotopic source signatures estimated from literature significantly underestimates true variability of source signatures. Source $\delta^{18}O$ signature was found to be the most sensitive tracer for urban/industry versus agricultural N_2O. $\delta^{15}N^{bulk}$ and site preference may provide more insight into microbial and chemical emission processes than partitioning of anthropogenic source categories.

1. Introduction

Nitrous oxide (N_2O) is the most important contributor to stratospheric ozone destruction emitted in the 21st century and one of the dominant anthropogenic greenhouse gases, with a global warming potential nearly 300 times higher than CO_2 [*Ravishankara et al.*, 2009; *Intergovernmental Panel on Climate Change (IPCC)*, 2013]. The mole fraction of tropospheric N_2O has increased from 270 ppb in preindustrial times to the current level of nearly 330 ppb, with an average growth rate of ~0.3% over the past decades [*Prinn et al.*, 2000, 2013; *Park et al.*, 2012; *Toyoda et al.*, 2013]. N_2O is long lived, with an estimated lifetime of around 116 ± 9 years [*Prather et al.*, 2015], and it is emitted from highly variable, disperse sources, which complicates efforts to quantify emission processes. Thus, novel techniques and approaches are needed to constrain the N_2O budget and facilitate the development of targeted mitigation strategies.

Monitoring the isotopic composition of N_2O, in addition to its mole fraction, may provide a useful constraint to quantify N_2O sources and improve our understanding of the N_2O budget [*Kim and Craig*, 1993; *Rahn and Wahlen*, 1997; *Toyoda et al.*, 2013]. The N_2O molecule has four common stable isotopic variants, also known as "isotopocules": $^{14}N^{14}N^{16}O$, $^{14}N^{14}N^{18}O$, $^{14}N^{15}N^{16}O$ (α), and $^{15}N^{14}N^{16}O$ (β). Therefore, not only the bulk isotopic composition ($\delta^{15}N^{bulk}$ and $\delta^{18}O$) but also the site-specific isotopic composition (site preference = $\delta^{15}N^{\alpha} - \delta^{15}N^{\beta}$) can be considered (see *Toyoda et al.* [2013] for a detailed description of notation and terminology). Previous studies indicate that the site preference (SP) is independent of substrate isotopic composition, and may be particularly useful to distinguish between microbial pathways at the laboratory and site scales [*Perez et al.*, 2001; *Sutka et al.*, 2006; *Wunderlin et al.*, 2012; *Harris et al.*, 2015a]. For example,

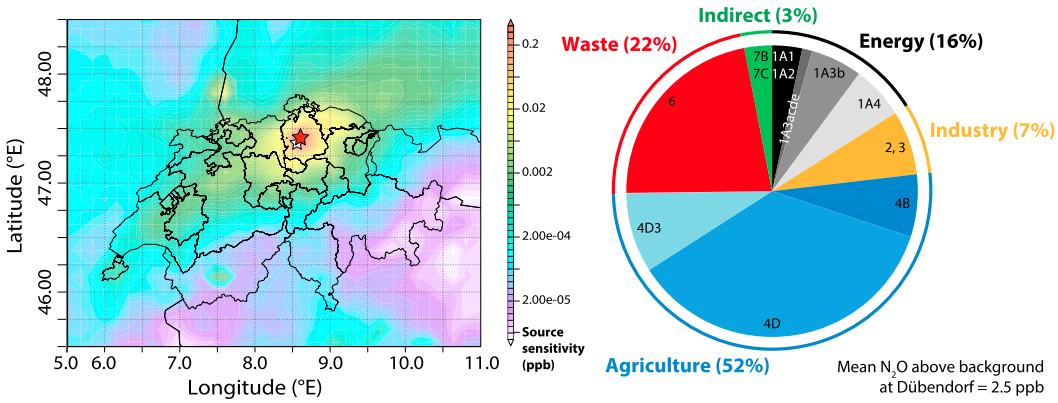

Figure 1. N_2O source contributions at the Dübendorf site. The left panel shows the annual mean source contribution in ppb for June 2014 to June 2015, calculated from FLEXPART-COSMO simulations multiplied by the total N_2O emission strength from Emissions Database for Global Atmospheric Research (EDGAR). The measurement site is indicated with a red star and the city of Zürich with a white star. The pie chart shows a breakdown of the annual mean N_2O above background at Dübendorf (2.5 ppb total) into EDGAR/Intergovernmental Panel on Climate Change (IPCC) source categories—these data are taken from the FLEXPART-COSMO + EDGAR simulations as described in sections 2.4 and 2.5.

the microbial N_2O-generating processes of NH_2OH oxidation and denitrification exhibit distinct SP values of 29 to 36 and −10 to 0‰, respectively [*Sutka et al.*, 2006; *Heil et al.*, 2014].

Recent developments in measurement techniques have allowed high-resolution time series of N_2O isotopic composition to be recorded using preconcentration coupled to a Quantum Cascade Laser Absorption Spectrometer (P-QCLAS) [*Mohn et al.*, 2012; *Harris et al.*, 2014; *Wolf et al.*, 2015]. QCLAS takes advantage of inherent differences in the fundamental rovibrational bands of N_2O isotopomers to directly measure the mole fractions of all four isotopecules of N_2O. In contrast to the more established technique of isotope ratio mass spectrometry (IRMS), P-QCLAS is cryogen-free and allows automated, online monitoring and field deployability, while maintaining high analytical precision [*Mohn et al.*, 2014].

N_2O isotope analysis with P-QCLAS opens new avenues of scientific enquiry regarding the N_2O budget. Similar analytical setups have been developed to measure in situ CH_4 isotopic composition [*Eyer et al.*, 2016; *Röckmann et al.*, 2016] and distinguish between different sources such as fossil fuel, biomass burning, and landfill based on unique isotopic signatures [*Snover et al.*, 2000; *Whiticar and Schaefer*, 2007; *Rigby et al.*, 2012]. The use of N_2O isotopocules to distinguish between anthropogenic source categories, such as soil, wastewater, and energy emissions, is, however, not well established, and isotopic ranges for source categories are poorly known [*Toyoda et al.*, 2013]. Compared to CH_4, the long atmospheric lifetime as well as the disperse and low-source-strength emission processes result in tiny variations in isotopic composition in ambient air, necessitating very high analytical precision and stability.

This study presents the first long-term, semicontinuous time series of N_2O isotopic composition, measured with P-QCLAS at a suburban site. Background and source isotopic composition are determined based on the measurement data. Auxiliary air quality and meteorological data are used to understand the factors controlling source isotopic composition and to consider the impact of different anthropogenic source types. Additionally, transport simulations are used to further investigate regional variability in N_2O sources, and to simulate N_2O isotopic composition using literature estimates of source isotopic signatures.

2. Methods

2.1. Site Description

Semicontinuous, online measurements of N_2O mole fraction and isotopic composition are conducted at the Empa campus in Dübendorf (432 m above sea level, 47°24′9″N, 8°36′43″E) from a rooftop air inlet located on the top of a five-storey building at a height of 13 m (Figure 1). Air is continuously sampled through a 25 m long unheated tube (Synflex 1300, ID 9 mm) at a flow rate of ~25 L min^{-1}. Measurements were made every 1–2 weeks over a 19 month period between July 2014 and February 2016, with data covering around 20% of the total time range (Figures 2 and S1 in the supporting information); during each intensive 2–6 day long sampling period, measurement time resolution is <1 h^{-1}. Additionally, measurements of air pollutants and

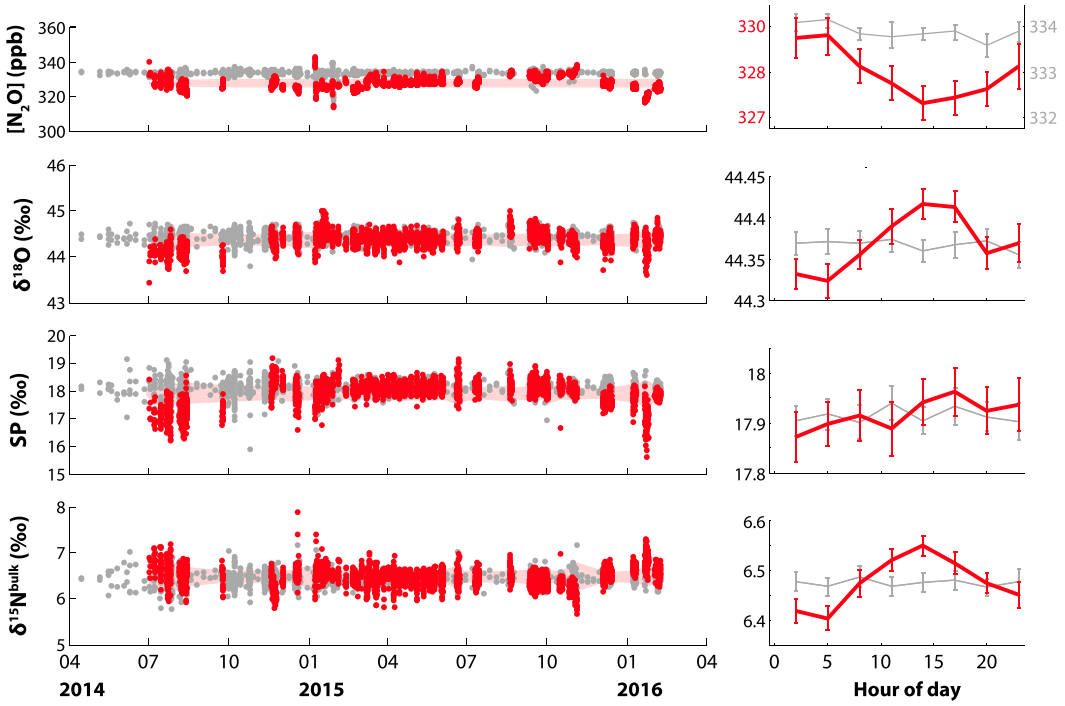

Figure 2. Time series of N_2O mole fraction and isotopic composition measurements made at Dübendorf using P-QCLAS. Ambient air measurements are shown in red and target gas measurements are shown in grey. Shaded red areas indicate the 1σ standard deviation of target gas measurements over 3 days, which offers the best approximation of the uncertainty of ambient air measurements. Right panels show the average diurnal cycle (3 h bins) over the entire measurement period with error bars indicating the 1σ standard deviation.

meteorology run continuously at the Dübendorf NABEL (National Air Pollution Monitoring Network) station, located on the Empa campus 110 m from the sampling inlet [*NABEL*, 2015].

Dübendorf lies within the Zürich agglomeration area, which has over 1.2 million inhabitants. The site is surrounded by a mix of suburban commercial, traffic, small-scale agricultural, and residential zones, with a significant number of busy roads and motorways in the immediate vicinity of the sampling site. The city of Zürich (population 380,000) is 7 km from Dübendorf toward the west/south west, and intensive agricultural land is located less than 10 km from the site, particularly toward the east [*Hotz and Weibel*, 2005].

2.2. Preconcentration of N_2O and Measurement of Isotopic Composition With QCLAS

The four most abundant N_2O isotopocules ($^{14}N^{14}N^{16}O$, 99.03%; $^{14}N^{15}N^{16}O$, 0.36%; $^{15}N^{14}N^{16}O$, 0.36%; $^{14}N^{14}N^{18}O$, 0.20%) are measured using a preconcentration system followed by a Quantum Cascade Laser Absorption Spectrometer (QCLAS; Aerodyne Research, Inc., USA). The setup has been described previously [*Mohn et al.*, 2010, 2012; *Wolf et al.*, 2015] and only a brief overview will be given here. Ambient air is sampled at a rate of 500 mL min^{-1} using a membrane pump (PM25032-022, KNF Neuberger, Switzerland). Upstream of the pump, sample air is dried using a permeation drier (PermaPure Inc., USA). Downstream of the pump, the air is passed through a second permeation drier, as well as Ascarite and Sofnocat 423 traps to remove CO_2 and CO respectively, before entering the preconcentration unit. A volume of 5.9 L of ambient air is collected on a HayeSep D trap at ~128 K (-145°C). During trapping, the temperature was always kept below 133 K, because N_2O desorption was measured to begin at temperatures > 135 K. Trapped N_2O is released into the 2.7 L absorption cell of the QCLAS by warming the trap to 0°C and flushing with synthetic air at a flow rate of 25 mL min^{-1} to a final cell pressure of 16.05 ± 0.04 hPa, resulting in a mole fraction of ~45 ppm N_2O.

Sampling is semicontinuous: Trapping takes 12 min, and a trapped sample is measured approximately every 35 min. The mole fractions of the four isotopocules are measured for 245 and 210 s, respectively, for trapped (sample and target) and standard gases. Potential fractionation introduced by trapping was determined by diluting a concentrated standard and passing it through the preconcentration unit to reconcentrate and comparing to the same standard measured directly. The fractionation effect was calculated before the

measurement period began, and no changes were made to the trapping procedure throughout the measurement period. The fractionation effect was found to be negligible compared to the measurement uncertainty (<0.1‰) for all isotopocules and is not corrected.

2.3. Calibration Strategy and Data Processing

To ensure the required accuracy and repeatability, several corrections and a two-point calibration are applied to all data. Additionally, repeated measurements of a tank of pressurized air, used as a target gas, are made to monitor repeatability and long-term instrumental drift, as described in *Mohn et al.* [2012] and *Wolf et al.* [2015]. Data processing is carried out using Matlab (MathWorks, Inc., USA). For all data processing as well as analyses and discussion throughout this paper, a threshold of $p < 0.05$ is used to test for significance unless stated otherwise. Data are collected, processed and corrected in intermittent periods of semicontinuous measurements spanning 1-6 days, within which time no changes were made to the instrumental set up or operation.

An anchor standard, S1, is used with isotopic composition close to ambient N_2O. The first step of data processing involves correcting all data according to the drift in S1, smoothed to a two-point moving average. Drift is due to numerous factors, including fluctuations in laboratory temperature and drift in laser emission power and frequency. Linear regression corrections for laser emission frequency drift, cell pressure, and N_2O mole fraction are then calculated based on S1 isotopic ratios. If the correlations for S1 are significant, the corrections are applied to all data. The correction for mole fraction is largest, averaging 0.07, 0.09, and −0.02‰ ppm^{-1} for $\delta^{15}N^{\alpha}$, $\delta^{15}N^{\beta}$, and $\delta^{18}O$, respectively, applied on an average standard deviation of 1.6 ppm for target gas in-cell N_2O mole fraction over the 19 month measurement period. Corrections for emission frequency drift and cell pressure are generally <0.05‰.

A second standard, S2, is used for two point calibration, with isotopic composition significantly lower than S1 in $\delta^{15}N^{\alpha}$, $\delta^{15}N^{\beta}$ and $\delta^{18}O$ (>35, 40, and 10‰ lower respectively). The two-point calibration is calculated based on S1 and S2 isotopic composition and applied to all data. As there is no international primary isotopic standard available for N_2O, we use standards calibrated by the Tokyo Institute of Technology [*Mohn et al.*, 2014], using their analytical technique as a link to the international scales [*Toyoda and Yoshida*, 1999]. An extensive intercomparison campaign conducted in 2013–2014 showed excellent agreement between Empa and Tokyo Tech N_2O isotope measurements [*Mohn et al.*, 2014]. A further intercomparison of four compressed air tanks conducted between November 2015 and January 2016 confirmed the ongoing close linkage between the isotope scales of the two laboratories (unpublished data).

The repeatability of isotopic data was considered based on the repeated measurements of target gas made over the 19 month measurement period. Four different target gases were used, for 4, 3, 9, and 3 months, respectively, through the 19 month measurement period. A total of 1778 target gas measurements were made, and these were split into two data sets: Two of every three measurements were designated as "target gas standards" (hereafter "T1"), while every third target gas was not used to calculate any corrections and therefore considered a robust measure of repeatability (hereafter "target gas"). T1 was used to calculate and correct for longterm drift in target gas and samples, following the principles of identical treatment [*Werner and Brand*, 2001]. A gradual decrease of 0.5‰, 0.5‰, and 0.4‰ was seen in T1 $\delta^{18}O$, SP and $\delta^{15}N^{bulk}$ over the entire 19 month period (Figure S1 in the supporting information)—this drift is despite the fact that measurements were anchored using the two-point calibration described above. Reasons for the gradual shift might be instrumental changes, variations in gas matrix (e.g., oxygen content) of T1 caused by different cylinders of synthetic air used for desorption or incomplete separation of oxygen during N_2O preconcentration. Gravitational separation of isotopocules in high-pressure tanks could potentially occur; however, correlation between long-term drift in T1 and drift in samples suggests an instrumental cause. All data were therefore corrected using a 10 day smoothed difference of each T1 measurement from the mean T1 value—a 10 day window was chosen to gain a balance between the level of drift and the standard error of repeated target gas measurements. To allow comparison of repeatability between the four different target gases, the target gas results were also normalized to the most recent target gas. The raw and the corrected and normalized results are shown in Figure S1.

Ambient N_2O mole fractions are calculated from analyzed preconcentrated N_2O mole fractions by applying a one-point calibration using S1, as well as a correction based on measurements of T1. The one-point calibration using the measured mole fraction and the known dilution factor for S1 is first applied to the data, to account for slight sensitivity changes of the spectrometer. Then approximate atmospheric equivalent mole fractions of T1,

target gas, and sample gas are calculated from measured data using the trapped volume (5937 ± 77 mL), gas pressure (16.05 ± 0.04 hPa) and cell volume (~2.7 L). Finally, the results are calibrated to the National Oceanic and Atmospheric Administration/Global Monitoring Division (NOAA/GMD) scale (WMO-N2O-X2006A) using the known mole fractions for T1, which are measured in the Global Atmospheric Watch World Calibration Centre (GAW-WCC) laboratory at Empa against a set of three NOAA/GMD reference standards on an Aerodyne QCLAS instrument (CO and N_2O monitor, Aerodyne Research, Inc., USA).

2.4. Modeling With FLEXPART-COSMO

The Lagrangian Particle Dispersion Model (LPDM) FLEXPART [*Stohl et al.*, 2005] was coupled to the numerical weather forecast model COSMO [*Baldauf et al.*, 2011] to provide emission sensitivities ("footprints") based on the residence time of virtual particles in a surface layer [*Seibert and Frank*, 2004]. These emission or source sensitivities illustrate the direct influence emissions from a source location would have on the mole fraction at the receptor site. The FLEXPART model setup is identical to that described by *Henne et al.* [2016]. The model has a resolution of ~7 × 7 km over Europe (36.06–57.42°N, −11.92–21.04°E). Four-day backward trajectories were calculated for 50,000 particles released every 3 h from 12 m height at the Dübendorf site.

The Emissions Database for Global Atmospheric Research (EDGAR) [*Olivier et al.*, 1994; *JRC/PBL*, 2009] provides greenhouse gas emissions on a 0.1° grid. The EDGAR emission inventory v4.2_FT2010 was used as an emission estimate, to calculate N_2O source contributions (in ppb) at Dübendorf, by multiplying with the FLEXPART source sensitivities. Therefore, we use the three hourly emission sensitivities from FLEXPART-COSMO, multiply with the EDGAR emission estimates, and integrate over space and time, to simulate the total N_2O source contributions to Dübendorf (i.e., the N_2O picked up in the 4 days prior to arrival at Dübendorf), and the contribution of individual EDGAR source categories to total emissions. The mean source contribution and the mean contribution from each category for the Dübendorf site are shown in Figure 1.

Four collocated category groups were defined from the 13 categories included in the EDGAR database for N_2O. These groups were selected to account for roughly equal fractions of the total source contribution and to reflect similar source distributions (e.g., point versus disperse and urban versus rural) and emission types: waste (IPCC emission categories 4B +6), energy/industry (hereafter "Energy" 1 + 2 + 3 + 4F), direct soil emissions (4D), and indirect soil emissions (4D3 + 7). These four groupings are used throughout this manuscript to simplify data analysis and visualization compared to considering all 13 categories.

2.5. EDGAR Emission Estimates: Temporal Variability and Isotopic Composition of Different Source Categories

EDGAR country total emissions for Switzerland are generally in agreement with the Swiss emissions reported to United Nations Framework Convention on Climate Change (UNFCCC) although certain categories deviate, e.g., agricultural emissions are higher in the Swiss inventory [*Federal Office for the Environment (FOEN)*, 2016] (Figure S2 in the supporting information). Bottom-up studies show natural emissions in Switzerland are negligible compared to indirect anthropogenic emissions induced by increased N deposition, which are covered under categories 4D3 and 7 in the EDGAR inventory [*Bühlmann et al.*, 2014, 2015; *Vitousek et al.*, 2013; *Carter et al.*, 2012]. In agreement, top-down inversion studies, utilizing atmospheric N_2O observations and transport simulations, have found that natural sources across Europe contribute very little N_2O compared to direct and indirect anthropogenic sources [*Bergamaschi et al.*, 2015]. In addition to their small magnitude, natural sources exhibit high spatial and temporal variability which is difficult to represent without a complex land model [*Bouwman et al.*, 1995; *Stehfest and Bouwman*, 2006]. Natural sources were therefore not considered in this study.

Previous inverse modeling studies have found that the EDGAR database is relatively accurate for total N_2O emissions in Europe with no large biases evident [*Bergamaschi et al.*, 2015; *Thompson et al.*, 2014b]. However, the partitioning between source categories is highly uncertain; in addition, N_2O emissions can be expected to exhibit significant temporal variability which is not included in EDGAR. Therefore, seasonal variability of the major source categories was defined using data and statistics for Switzerland, as north-east Switzerland was found to be the main origin of transport footprints for Dübendorf (Figure 1). Isotopic composition ranges for the different EDGAR source categories were estimated based on published literature data, to allow construction of a simulated a priori time series of mole fraction and isotopic composition covering the measurement period. Categories are discussed using the category names from the EDGAR inventory; a detailed description is given in the supporting information (Text S1), and the results are summarized in Table 1.

Journal of Geophysical Research: Atmospheres

10.1002/2016JD025906

Table 1. Summary of Spatial Allocation, Seasonality and Isotopic Composition of Major Anthropogenic N_2O Sources[a]

Categories	Primary Source(s)	Spatial Allocation	Seasonal Variability	$\delta^{18}O$	$\delta^{15}N^{bulk}$	SP	References
1A1 and 1A2	$deNO_x$ use in fossil fuel and MSW incineration plants	Point sources (population)	None	35.9 ± 13.1	3.9 ± 2.9	17.6 ± 0.5	1, 2
1A3a, 1A3c, 1A3d, 1A3e	Fuel combustion in nonroad transportation	Population, ship traffic density (point sources)	Summer peak	28.6 ± 9.9	-28.7 ± 3.6	4.2 ± 2.4	3
1A3b	Fuel combustion for road transportation	Road density	Summer peak	40.3 ± 3.7	-7.2 ± 1.2	10.0 ± 4.3	3
1A4	Fuel combustion: Other sectors (dominantly household heating)	Population	Winter peak	37 ± 10	5.5 ± 6	3.5 ± 4	1, 4
2 and 3	Nitric acid production (adipic acid, medical, and private (aerosol) use)	Point sources (population)	None	29.1 ± 18.8	-8.3 ± 10.6	3.3 ± 5.5	3, 5, 6
4B	Manure management	Animal density	None ($[NO_2^-]/[NO_3^-]$)	23.9 ± 3.8	-17.5 ± 6.2	6.5 ± 4.1	7
4D	Direct soil emissions	Cropland and soil maps	NA	29.0 ± 3.7	-17.8 ± 5.7	7.2 ± 3.8	8, 9
4F	Agricultural waste burning	Cropland map	NA	25 ± 3.0	-1.0 ± 3.0	2.8 ± 3.0	4
6	Waste (wastewater treatment)	Population	None ($[NO_2^-]/[NO_3^-]$)	31.5 ± 14.1	-11.6 ± 12.7	10.5 ± 5.7	8
4D3, 7B, and 7C	Indirect soil emissions	Cropland and soil maps	NA	29.0 ± 3.7	-17.8 ± 5.7	7.2 ± 3.8	8, 9

[a]EDGAR emission categories and the major process contributing N_2O in Switzerland. Spatial allocation refers to the proxy data used to distribute emissions in EDGAR. The seasonal variability and isotopic composition have been estimated from the literature as described in Text S1 in the supporting information. References: 1. *Ogawa and Yoshida* [2005b]; 2. *Harris et al.* [2015b]; 3. *Toyoda et al.* [2008]; 4. *Ogawa and Yoshida* [2005a]; 5. *Thiemens and Trogler* [1991]; 6. personal communication; S. Toyoda, TiTech; 7. *Maeda et al.* [2010]; 8. *Snider et al.* [2015]; and 9. *Wolf et al.* [2015].

Table 2. N_2O Mole Fraction and Isotopic Composition in Dübendorf, Switzerland[a]

	Mixing Ratio (ppm)	$\delta^{18}O$ (‰)	SP (‰)	$\delta^{15}N^{bulk}$ (‰)
		This Study		
Mean	328.0 ± 3.6	44.37 ± 0.18	17.92 ± 0.45	6.47 ± 0.23
Mean background	325.8 ± 3.3	44.41 ± 0.13	17.95 ± 0.40	6.53 ± 0.14
Trend ($year^{-1}$)	0.73 ± 0.3	0.17 ± 0.02	0.35 ± 0.04	−0.03 ± 0.02
Diurnal Cycle	1.39 ± 0.28	−0.09 ± 0.01	−0.07 ± 0.03	−0.12 ± 0.02
		Hateruma Island, Japan		
Mean		44.21	18.44	6.65
Trend ($year^{-1}$)	0.72	0.016 ± 0.007	−0.050 ± 0.027	−0.023 ± 0.006

[a]Summary of N_2O mole fraction and isotope composition from measurements made between July 2014 and February 2016 at the Empa campus in Dübendorf, Switzerland. Errors are the 1σ standard deviation. Diurnal cycle refers to the difference between nighttime (maximum mole fraction; 01:00–06:00) and daytime (minimum mole fraction; 13:00–18:00) average values. Mean values and trends from *Toyoda et al.* [2013] for a decadal time series measured in flask samples between 1999 and 2010 at a background site (Hateruma Island, Japan) are shown for comparison. The trends from Dübendorf should be regarded with caution, since the shortness of the time series, interannual meteorological variability, and the location of the site close to considerable emissions may have strongly influenced the estimate.

3. Results

3.1. Repeatability and Accuracy

The repeatability of target gas measurements (Figure S1) improved throughout the measurement period as various advances were made with the instrumentation, such as the installation of a new laser source (28 October 2015) and a temperature control system on the QCLAS electronics (20 January 2016). Thus, the 3 day standard deviation of repeated target gas measurements improved from 0.13‰, 0.33‰, and 0.22‰ in the first month of measurements to 0.08‰, 0.11‰, and 0.10‰ for $\delta^{18}O$, site preference, and $\delta^{15}N^{bulk}$, respectively, in the final month. The long-term drift correction from T1 (see section 2.3) was less than 0.10‰ for all delta values in the final months.

The repeatability of N_2O mole fraction data ranges from 0.2 to 1.6 ppb (3 day standard deviation of target gas) over the 19 months of measurement, due to changes and random variability in the trapping procedure and the instrumentation that were not captured in the calibration. The repeatability generally improved, averaging around 1.1 ppb at the start and 0.6 ppb at the end of the measurement period. The added complexity of the trapping and correction back to atmospheric mole fraction means the precision is lower than conventional online gas chromatography with electron capture detector (GC-ECD), Fourier transform infrared, or QCLAS analysis (<0.1–0.3 ppb precision [*Rapson and Dacres*, 2014]). To investigate linearity and accuracy of mole fraction measurements, we ran a 5 day intercomparison between the P-QCLAS technique and a QCLAS without preconcentration in the Empa GAW-WCC lab (CO and N_2O monitor, Aerodyne Research, Inc., USA). The average difference between the two techniques was 0.44 ± 0.42 ppb; thus, the two instruments agreed very well, particularly considering a slight time offset because the conventional QCLAS measures continuously while the P-QCLAS set up integrates over the trapping time. Both instruments reproduced the diurnal cycle over 5 days—which ranged in magnitude between 2 and 6 ppb—with a slope of 0.89 and R^2 of 0.88 between the two analytical techniques (Figure S3).

3.2. Variability in Measured N_2O Mixing Ratio and Isotopic Composition

The time series of mole fraction and isotopic composition of N_2O measured at Dübendorf is shown in Figure 2 and summarized in Table 2. The mean mole fraction (328.9 ± 3.6 ppb) is above the mean Northern Hemisphere (NH) background value of 327.6 ± 0.2 ppb for the same time period (Advanced Global Atmospheric Gases Experiment network data [*Prinn et al.*, 2013, 2000; *Thompson et al.*, 2014a]), as Dübendorf is a suburban site. The observed trend for all data of 0.73 ± 0.3 ppb yr^{-1} in N_2O mole fraction is in good agreement with the result of 0.72 ppb yr^{-1} for Hateruma Island, Japan [*Toyoda et al.*, 2013], as well as the Northern Hemisphere mean trend for the last 5 years of 0.94 ± 0.02 ppb yr^{-1} [*Prinn et al.*, 2013, 2000; *Thompson et al.*, 2014a]. The isotopic trends are much larger than observed previously [*Toyoda et al.*, 2013], which may be due to seasonality and/or interannual variability in isotopic composition and magnitude of the regional source.

However, the mole fraction and isotopic trends from Dübendorf should be regarded with caution, since the shortness of the time series, interannual meteorological variability, and the location of the site close to considerable emissions may have strongly influenced the estimate.

The data show significant diurnal cycles in N_2O mole fraction, $\delta^{18}O$, SP, and $\delta^{15}N^{bulk}$ (Figure 2), corresponding to the nighttime buildup of isotopically depleted N_2O emitted into the boundary layer on top of the isotopically enriched tropospheric background. The mean source isotopic signature at Dübendorf was estimated with a Keeling plot approach using a weighted fit to the mean diurnal data [*Keeling*, 1958, 1960] to be 26.0 ± 8.5‰, 5.4 ± 13.0‰, and −21.6 ± 10.1‰ for $\delta^{18}O$, SP, and $\delta^{15}N^{bulk}$, respectively, (R^2 = 0.91, 0.71, and 0.94). Variability in source isotopic composition will be discussed in detail in sections 3.4 and 3.5.

The mean diurnal cycle of N_2O mole fraction at Dübendorf is 1.4 ppb, and changes of >5 ppb within 24 hours are common. The diurnal cycle in isotopic composition, however, is rarely more than ~0.5-0.8‰ and averages ~0.1‰ (Table 2) for all isotopocules. In contrast, at a near-surface managed grassland site, *Wolf et al.* [2015] only determined source isotopic composition when the overnight build up of N_2O was >12 ppb - changes of this magnitude are rarely seen at Dübendorf. Measurement precision of ~0.1‰ is therefore clearly needed to observe changes in isotopic composition at urban and suburban sites; it can be expected that even higher precision is required for the more remote sites and towers typically used in inversion modeling studies considering regional-scale sources.

3.3. Determining N_2O Background From Measurement Data

The measurements at Dübendorf can be considered as a combination of regional to local scale sources imposed upon a slow-moving background. An estimate of the background is therefore needed in order to determine the source isotopic composition contributing above background N_2O (as described in the next section). Furthermore, in order to compare the measurements to the FLEXPART-COSMO/EDGAR model results, the larger-scale background mole fraction which is not accounted for by the model is required — this corresponds to N_2O in the air parcel before it enters the spatiotemporal model domain. We therefore attempted to estimate the background from the observations, assuming that at times the sampled air was not significantly influenced by recent emissions. The minimum 5% of mole fraction data points in a moving 10 day window were flagged to represent this background. The isotopic baseline was determined by averaging the isotopic values of the flagged background points and smoothing over a 10 day window. The flagged and final smoothed backgrounds are shown in Figure S4. Varying the cutoff value to between 5 and 20% of mole fraction data, or the size of the window between 5 and 15 days, did not affect the background within the uncertainty limits (±0.5 ppb or 0.15‰). Uncertainty in the background mole fraction and isotopic composition, defined as a running standard deviation, is propagated into all following calculations.

The mean background isotopic values are 44.41 ± 0.13‰, 17.95 ± 0.40‰ and 6.53 ± 0.14‰ for $\delta^{18}O$, SP, and $\delta^{15}N^{bulk}$, respectively. These results agree well with background air measurements at Hateruma Island [*Toyoda et al.*, 2013] when the results from *Toyoda et al.* [2013] are extrapolated to 2015 (Table 2; no published background site measurements are available for 2015). Isotopic composition moved both above and below the background; however, the mean and median shifts from baseline were negative for all isotopocules, corresponding to isotopically light sources. The distributions of shifts from the baseline were not normal but skewed toward negative values for all isotopocules (Figure S4), because the tropospheric background is isotopically heavier than the mean source to balance the backflux of isotopically heavy N_2O from the stratosphere [*Rahn and Wahlen*, 1997; *Kaiser et al.*, 2002; *Toyoda et al.*, 2004].

3.4. Mixing Model to Determine the Integrated Source Isotopic Signature

The isotopic composition of the integrated total sources contributing N_2O above background was estimated from the observations at Dübendorf (hereafter referred to as "measured source" isotopic composition). Typically, a Keeling plot approach is used to find source isotopic composition [*Keeling*, 1958, 1960; *Wolf et al.*, 2015; *Röckmann et al.*, 2016; *Vardag et al.*, 2016]. However, for N_2O in ambient air, changes in mole fraction are very small, and thus, extrapolation to the intercept of $(\text{mole fraction})^{-1}$ results in large uncertainties. The Keeling plot method assumes both the source and background remain constant through the time window over which the fit is calculated; an assumption that cannot be easily justified [*Vardag et al.*, 2016]. Additionally, the background uncertainty cannot be explicitly considered in the Keeling plot approach. Therefore, a different method was used to find the source isotopic composition.

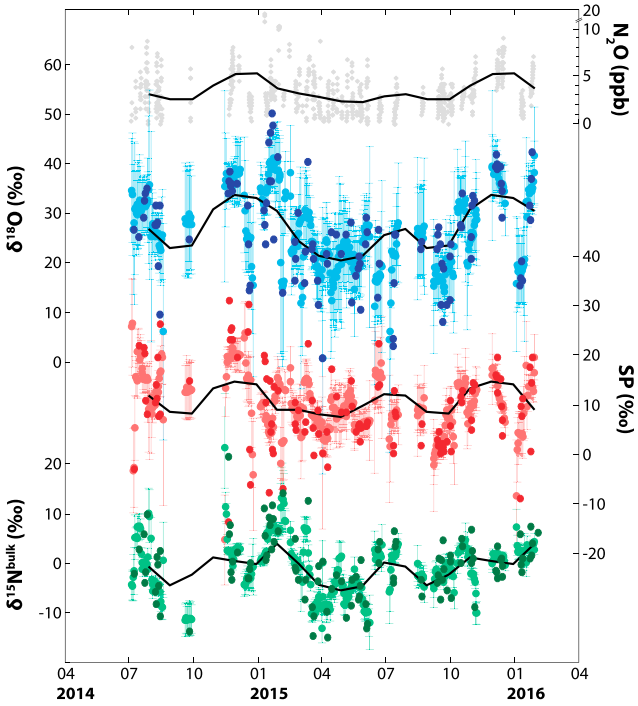

Figure 3. One day (dark) and 5 day (pale points) moving mean source isotopic composition calculated from measured data using equation (2); data are only shown where the regression was significant, as described in section 3.4. The error bars (for 5 day values) show the 1σ uncertainty. The mean seasonal cycles are shown with black lines. The measured data points and mean seasonal cycle in above background N_2O is also shown for comparison.

The measured isotopic composition δ_m is a function of the background isotopic composition δ_b and the isotopic composition of the integrated total sources of N_2O (δ_s):

$$\delta_m = f_b \times \delta_b + \Sigma\left(f_s \times \delta_s\right) \quad (1)$$

where f is the mass fraction of N_2O from the background (b) and the sources (s; i.e., above background N_2O). Due to the long lifetime of N_2O, stratospheric sink processes are implicitly included in the background. The isotopic composition of the integrated sources can therefore be found from the measured mole fraction and isotopic composition and the background mole fraction and isotopic composition, as the slope of the fit

$$\delta_m - \frac{C_b}{C_m} \times \delta_b = \frac{C_m - C_b}{C_m} \times \delta_s \quad (2)$$

where C_m is the measured mole fraction and C_b is the N_2O mole fraction in background air; similar to the approach detailed by *Miller and Tans* [2003]. This method assumes that the source isotopic composition remains constant over the time window of the calculation, while the background is allowed to vary, and the uncertainty in the background can be explicitly considered. This assumption is difficult to test; however, the simulation indicates that there are no significant diurnal changes in the fraction of N_2O from different source types reaching Dübendorf over the measurement period (comparison of mean values for 04:00 to 07:00 and 16:00 to 19:00; $p \ll 0.01$).

The measured source isotopic composition was determined for moving windows of 1 or 5 days, starting at 16:00 each day to coincide with the minimum N_2O mole fraction. Only windows with at least five data points and a fit significance for equation (2) of $p < 0.05$ were used. The individual error in mole fraction and isotopic composition for each measurement and background point was assumed to follow a normal distribution and used to find the error in the measured source isotopic composition following 200 iterations of equation (2) for a Monte Carlo uncertainty approximation; as covariance was not considered the uncertainty estimates may be at the lower limit. Both 1 and 5 day windows were considered to give a balance between temporal resolution, number of data points in each fit, and uncertainty in the measured source isotopic composition: With time windows shorter than 1 day, the uncertainty is too high for useful results, and for windows longer than 5 days, the uncertainty improves very little and true temporal variability is lost. As stated in the previous subsection, the background estimation method (i.e., time frame, cutoff between 5% and 20%) did not affect the calculated background outside the uncertainty limits—as the background uncertainty is propagated in equation (2), the background estimation method also has no significant impact on resultant source isotopic composition. The mean uncertainties in the source isotopic compositions were 7.9‰, 4.1‰, and 1.9‰ for 5 day and 14.2‰, 7.3‰, and 3.5‰ for 1 day fits $\delta^{18}O$, SP, and $\delta^{15}N^{bulk}$, respectively, with an average buildup of N_2O above background of 3.3 ppb (~1% of the total N_2O). In terms of uncertainty, the method performs significantly better than the Keeling plot approach to determine source isotopic composition, where ≥12 ppb N_2O above background was needed to determine source isotopic composition with similar uncertainty [*Wolf et al.*, 2015].

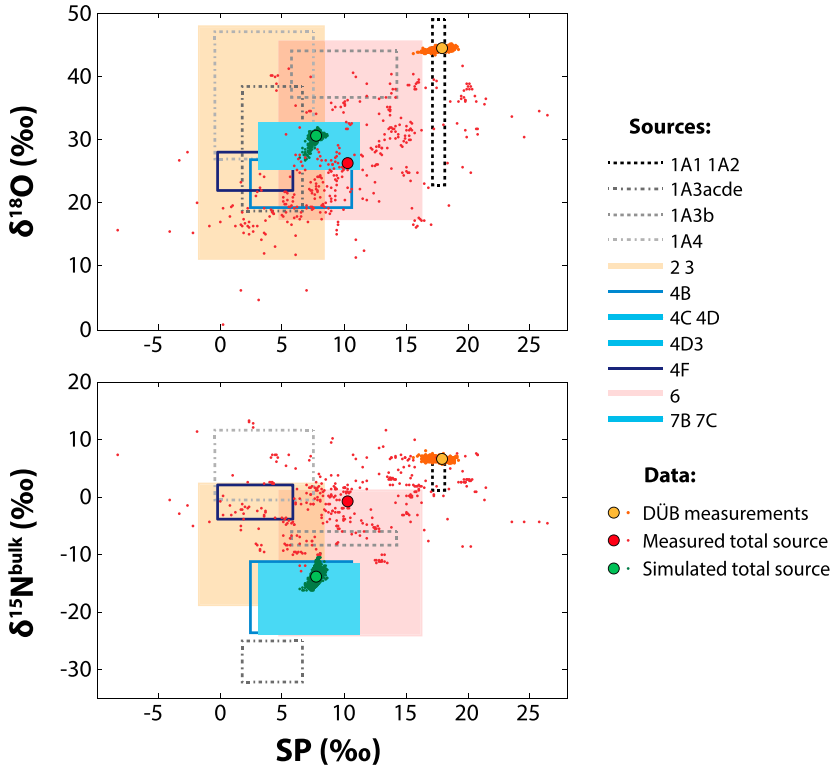

Figure 4. Isotopic composition of N_2O sources. Literature estimates of the range of isotopic signatures for different source categories are shown in the colors indicated in the legend; see Table 1 for details on the different categories. The ambient isotopic composition measured at Dübendorf is shown in orange, while the measured source isotopic composition calculated using equation (2) is shown in red. The simulated source isotopic composition, calculated using the literature source signatures, is shown in green. For the different data sets, individual values are shown as small dots and means are shown as large colored circles.

A time series of measured source isotopic composition is shown in Figure 3, with the mean seasonal cycle shown as a spline fit. Seasonal cycles (summer-winter difference) are significant at $p < 0.01$ for all isotopes. It can be seen that the 1 day and 5 day source isotopic compositions generally agree well and show the same seasonal cycle, whereby $\delta^{18}O$ and SP show a peak in winter and a smaller peak in summer. The seasonal cycle for $\delta^{15}N^{bulk}$ is similar, but the winter peak is much less pronounced. Two-isotope plots of 5 day source isotopic composition are shown in Figure 4, for comparison with the measured ambient isotopic composition and the isotopic signatures for sources estimated from literature. Both the literature estimated and measured source signatures are isotopically depleted compared to the ambient measurements; however, the range in measured source isotopic signatures is larger than the full range of previously estimated signatures including uncertainty. Causes of variability in source isotopic composition will be investigated further in the following sections.

3.5. Causes of Variability in Source Isotopic Composition

The relationships between measurements, 1 day mean measured source isotopic composition from equation (2) and 1 day binned values for various air quality and meteorological parameters measured at the Dübendorf NABEL station were investigated. Cross correlations are shown in Figure S5. As expected, strong positive correlations ($p < 0.01$ and $R^2 > 0.1$) can be seen between all the indicators of "energy/industry" pollution such as SO_2, NO_x, black carbon, and PM10. Considering the descriptive power of these pollution tracers, a "pollution index" was created from the normalized values for NO_x and CO:

$$PI_t = \left(\frac{NO_{x,t}}{NO_{x,max}} + \frac{CO_t}{CO_{max}} \right) / 2 \quad (3)$$

The pollution index can range between 0 and 1 with the highest values indicating the measurement points with the greatest impact from urban/industrial pollution. Strong negative correlations are seen between

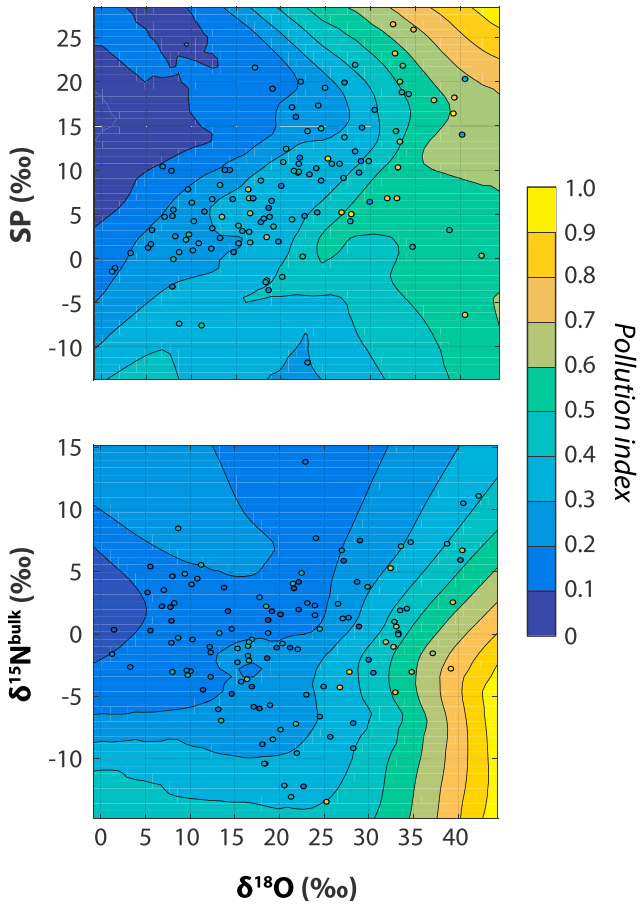

Figure 5. Two-isotope contour plots showing the relationship between N_2O 1 day measured source isotopic composition (from equation (2)) and pollution index (CO and NO_x). Individual measurement points are colored by pollution index, and contours represent a Lowess regression fit with a span of 30%.

these parameters and meteorological factors that are indicative of increased atmospheric dispersion, such as wind speed and temperature. Pollution tracers also correlate strongly with modeled source fraction from energy and waste and negatively with modeled source fraction from indirect and direct agricultural soil emissions. Overall, it can be seen that both the model and measurements at Dübendorf respond to times with a high influence of urban pollution and more stable meteorological conditions, compared to times when the air is more influenced by regional and larger-scale agricultural activities, when wind speed is higher and the site footprint is larger.

Above background N_2O strongly correlates with urban pollution tracers and pollution index ($p < 0.01$ and $R^2 > 0.1$), as stable meteorological conditions result in greater N_2O buildup—both for directly measured values, primarily due to diurnal cycles, and 5 day mean values, which reflect local and regional scale emissions and transport. Measured isotopic composition shows weak negative correlations with these tracers, reflecting the diurnal cycle, as the tropospheric mean N_2O is heavier than almost all anthropogenic sources (Figure 4) due to the backflux of isotopically enriched N_2O from the stratosphere [*Kaiser et al.*, 2002, 2006].

Two-isotope plots illustrating the relationship of measured source isotopiccomposition to pollution index are shown in Figure 5—these values are 5 day means and reflect local-/regional-scale transport and emissions, and not diurnal cycles. Isotopic composition of sources exhibits varying relationships to urban pollution, as indicated by the pollution index, for the different delta values. $\delta^{18}O$ shows a strong positive relationship with urban pollution ($p < 0.01$) while SP shows a weak positive trend (not significant at $p = 0.05$). $\delta^{15}N^{bulk}$ shows a weak but significant negative correlation ($p < 0.05$). These correlations are robust for almost all pollution tracers (Figure S5). The results therefore show that urban emissions from the city of Zürich are characterized by high-source $\delta^{18}O$ and low-source $\delta^{15}N^{bulk}$. For $\delta^{18}O$, this is in agreement with the previously estimated isotopic signature of the different source classes (Table 1 and Figure 4), whereby energy sources generally show relatively high $\delta^{18}O$ values. A low influence of local urban/industrial pollution implies a higher proportion of agricultural/soil emissions, as these are the major sources of N_2O globally and in Switzerland [*IPCC*, 2013; *FOEN*, 2016]. Thus, greater influence from soil emissions leads to depleted source isotopic composition for $\delta^{18}O$ and enriched source isotopic composition for $\delta^{15}N^{bulk}$. SP of emitted N_2O does not correlate significantly with pollution index, although a weak positive trend may be present (Figure 5). This suggests SP does not respond strongly to the importance of urban/agricultural sources, and other factors such as seasonally varying microbiological or abiotic emission pathways, or the proportion of biotic/abiotic N_2O reduction, may be of greater importance in determining SP than emission category. $\delta^{15}N^{bulk}$ shows a weak but significant negative correlation ($p < 0.05$). These correlations are robust for almost all pollution tracers (Figure S5).

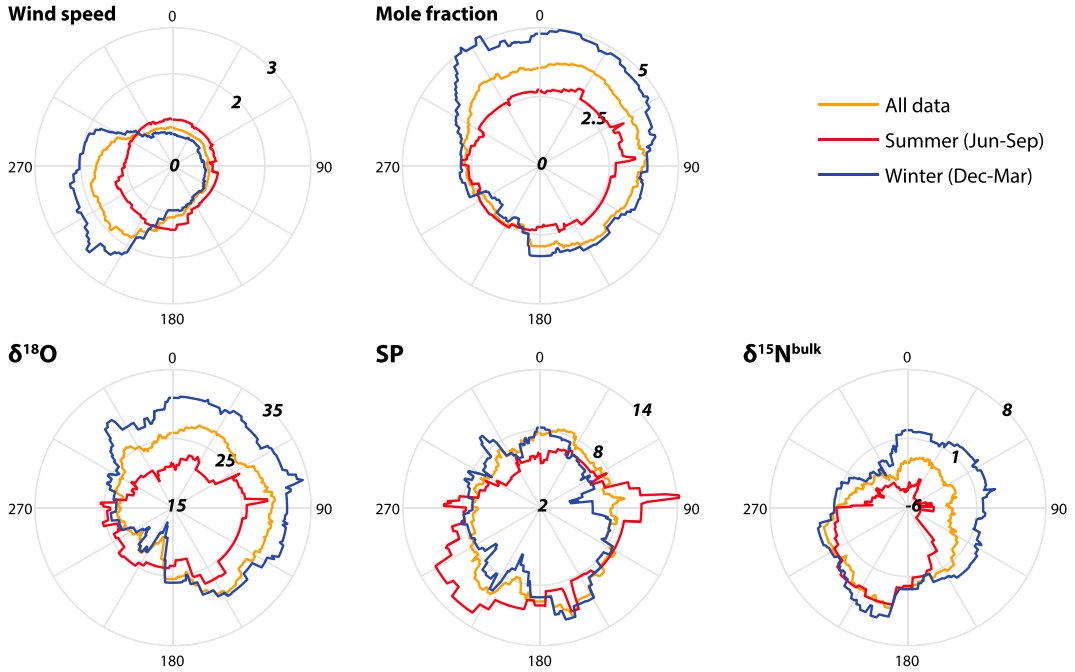

Figure 6. Dependence of wind speed, above background mole fraction and 1 day measured source isotopic composition (from equation (2)) on wind direction at Dübendorf. Mean values for all data and for summer (June–September) and winter (December–March) are shown for a moving 90° window.

For an in-depth understanding of temporal and spatial variability of soil N_2O processes and isotopic signatures, implementation of an isotope submodel in a biogeochemical soil model is required, which is beyond the scope of this study.

To further examine the effect of spatially varying emission sources—and thus meteorology and transport—on source isotopic composition, two approaches were considered: Using the local measured wind direction at Dübendorf and using the modeled site footprint. Both wind speed and footprint were considered, as the inlet of the Dübendorf measurement site is only 13 m above ground and located near potential emission sources; thus, the impact of subgrid cell processes could be significant. The influence of local wind direction on mean wind speed, N_2O mole fraction and measured source isotopic composition is shown in Figure 6. The simulated site footprint was considered using a transport cluster analysis (analogous to that presented by *Pandey Deolal et al.* [2014]); footprints were categorized into one of four clusters (Figure S6) representing SW (1), local (L, 2), W (3), and NE (4) transport. Mean measured source isotopic composition, NO_x, CO, CH_4, and wind speed for each cluster is shown in Figure 7.

The wind direction analysis shows that the strongest winds are from the southwest, particularly in winter, due to a well-known flow channeling between the Alps and Jura mountains [*Wanner and Furger*, 1990]. Consequently, N_2O mole fraction builds up to greater levels when slower northeasterly winds affect the site. The cluster analysis similarly shows a clear distinction in winter between cluster 3 (W), which is dominated by westerly flow and results in cleaner conditions (lower NO_x, CO, and CH_4), and the other clusters. In summer, the influence on the site is more localized, and there is less difference between clusters and wind directions. Both analyses show a significant dependence of measured source isotopic composition on the footprint of air reaching the site; for example, particularly high $\delta^{18}O$ for NE wind sector (0–90°) in winter can be clearly seen in Figure 6. Source $\delta^{18}O$ is 5–15‰ higher for clusters 1 (SW), 2 (L), and 4 (NE), and for wind directions between 270 and 180°, especially in winter. SP shows a similar but much weaker pattern in winter. $\delta^{15}N^{bulk}$ is highest for clusters 3 (W) and 4 (NE) in both summer and winter and around 5‰ higher in winter than in summer.

Considering the relationships between isotopic composition and urban pollution, as well as the wind direction and footprint cluster analyses, three regimes can be considered for N_2O at Dübendorf:

1. When the site is influenced by "clean" air (cluster 3 (W) or strong southwesterly winds), source $\delta^{18}O$ is low and $\delta^{15}N^{bulk}$ is high, and concentrations of pollution tracers are low. SP is low in winter and higher

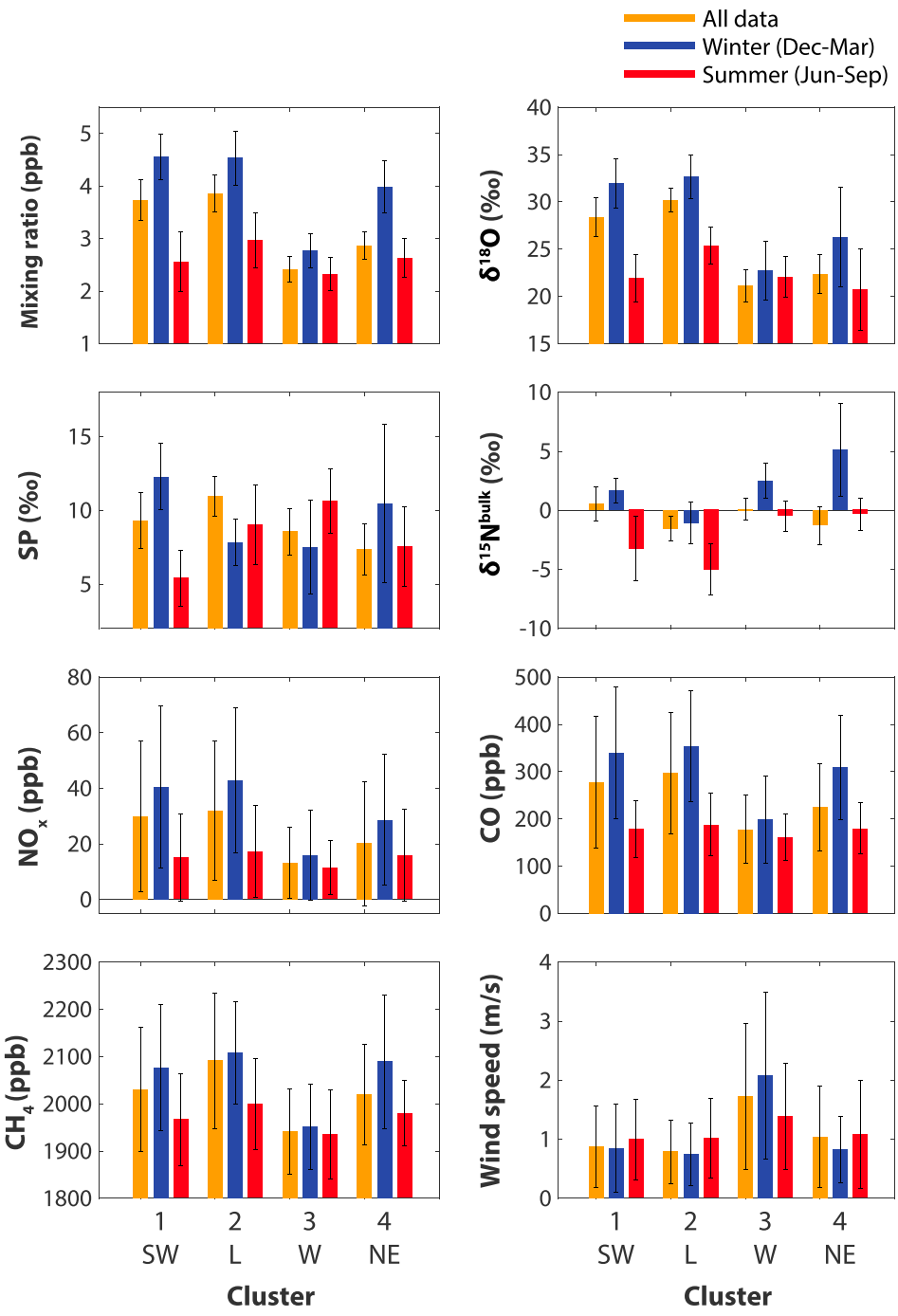

Figure 7. Mean values for different parameters for four footprint clusters over the whole measurement time period and for summer (June–September) and winter (December–March). Isotopic values are the measured source isotopic composition. Error bars are the 1σ standard deviation. Cluster footprints are shown in Figure S6; in brief, clusters represent transport from the southwest (SW), local (L), west (W), and northeast (NE) for 1–4, respectively.

in summer. The influence of clean air is particularly noticeable in winter, when wind speeds reach much higher values.

2. Clusters 1/2 (SW/L) and low daytime wind speeds, especially in summer, characterize a local and southwesterly regional influence on N_2O measured at the site. Concentrations of pollution tracers are high, $\delta^{18}O$ is high, and $\delta^{15}N^{bulk}$ is low. Source $\delta^{18}O$, SP, and $\delta^{15}N^{bulk}$ are higher in winter than in summer.

3. The site can be strongly affected by northeastern Swiss/European sources, described with cluster 4 (NE) and wind direction between 0 and 90°. $\delta^{15}N^{bulk}$ is highest in this regime in winter, while $\delta^{18}O$ is relatively low. SP is higher and $\delta^{15}N^{bulk}$ is much higher in winter than summer. Pollution tracer levels are moderate.

3.6. Modeling N_2O Mole Fraction and Isotopic Composition

3.6.1. Modeling N_2O Mole Fraction

The FLEXPART-COSMO transport model and modified EDGAR inventory as described in sections 2.4 and 2.5 were used to simulate above-background N_2O mole fractions. The total source contribution at Dübendorf and the contributions from different source categories are shown in Figures 1 (annual mean) and 8 (time series). The model results show that majority of above background N_2O measured at the site is from the city of Zürich and northeast Switzerland, with little transport across the Alps from Northern Italy. About 52% of above background N_2O is expected to be emitted by agriculture, with wastewater treatment (~22%) and energy production (~16%) also contributing significantly.

The simulated time series (representing only N_2O emissions picked up within the last 4 days prior to arrival at Dübendorf) was compared to the observed above background N_2O mole fractions (Figure 8). The simulation and observations show moderate agreement with $R^2 = 0.34$ considering the relatively high measurement uncertainty and the small size of peaks ($p \ll 0.01$) using the seasonally adapted emissions (see Text S1), compared to 0.28 for emissions without seasonality ("seasonality" and "no seasonality," respectively, in Figure 8). The agreement between the simulation and observations was significantly improved ($p<<0.01$) by adding seasonality to the simulated emissions. The mean residual (observations − simulation) for no seasonality was 0.69 ppb and the mean residual with "seasonal" emissions was 0.56 ppb. The mean diurnal cycle was somewhat underestimated in the model, resulting in a slope of 0.55 between the simulation and the observations, and reflecting the model's difficulties in correctly representing the concentration buildup in the nighttime stable boundary layer. The agreement is best between 15:00 and 21:00, with $R^2 = 0.52$ and a slope of 0.83 (Figure S7).

The significant seasonality in mole fraction, with higher mole fractions above background measured in winter, is primarily driven by meteorology and captured well by the model ($R^2 = 0.93$, slope = 1.01 for mean monthly mole fractions). The seasonality added to the EDGAR prior emissions affects only categories 1A3 and 1A4—which account for 15% of the total emissions measured at Dübendorf—while for the remaining categories (primarily soils and wastewater treatment) no seasonal variability was assumed. This leads to an overall seasonal variation of <5% in the total emissions. The good agreement between simulated and measured seasonal mole fractions (Figure 8) therefore suggests that there is little seasonality in the remaining emission categories. It is possible that the model has a seasonal bias; however, there are no significant seasonal differences evident in model performance (Figure S7), suggesting that the model captures summer and winter conditions similarly well. In contrast to our results, *Thompson et al.* [2011] found significant seasonality of ~50% in total N_2O fluxes in southern Germany using an inversion approach with continuous tall tower measurements made at Ochsenkopf, around 350 km northeast of Dübendorf. Microbial process emissions respond to seasonal factors such as temperature and soil moisture and also a range of other parameters, such as pH, substrate availability, fertilizer application and type, grazing, tillage, crop type, and freeze-thaw cycles [*Bouwman et al.*, 1995; *Bouwman*, 1996; *Smith et al.*, 1998; *Six et al.*, 2002; *Amon et al.*, 2006; *Owen and Silver*, 2014; *Wolf et al.*, 2010]—therefore, it is not unexpected that seasonalities differ at different sites. Interannual and/or spatial differences between N_2O fluxes and flux seasonal cycles are likely larger in magnitude than the seasonal cycles themselves. Long-term measurements are currently too sparse, and no emission/transport models have been published with the required degree of detail and accuracy, to judge the significance of this discrepancy.

3.6.2. Simulating N_2O Isotopic Composition

N_2O isotopic composition at Dübendorf was modeled by multiplying the contributions from each source to the total simulated N_2O at Dübendorf with the isotopic composition of the source:

$$R^X_{N_2O} = \frac{\sum C_i \times R^X_i + C_b \times R^X_b}{\sum C_i + C_b} \quad (4)$$

where $R^X_{N_2O}$ is the simulated change in isotopic composition of N_2O from the background due to the sources expressed as an isotope ratio ($R^X = \frac{[X]}{[Y]}$ where X and Y are the heavy and light isotopic variants, respectively, e.g., ^{18}O and ^{16}O); C_i is the mole fraction contribution of source i from the FLEXPART-COSMO + EDGAR

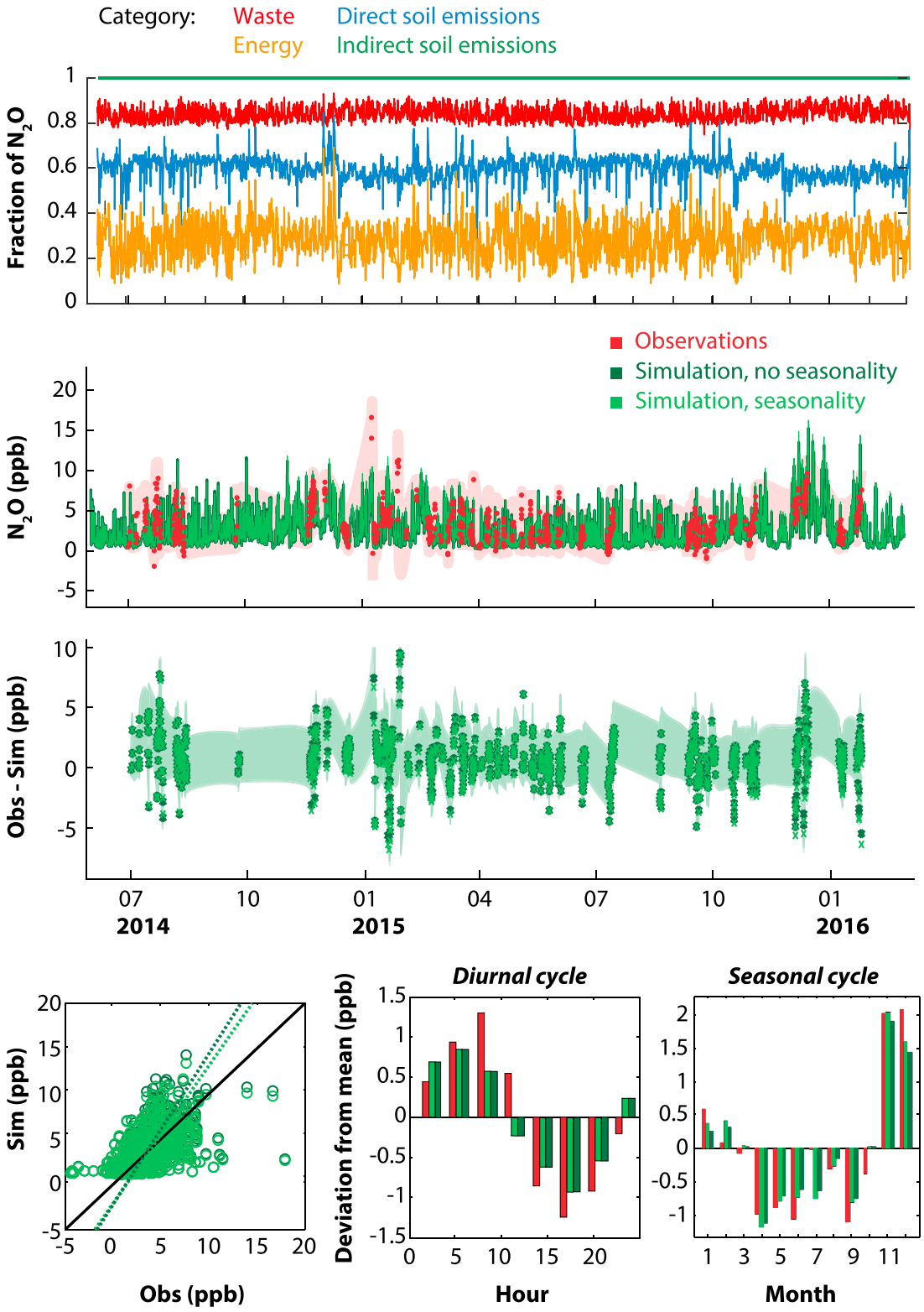

Figure 8. Comparison between observed and simulated N_2O mole fractions at Dübendorf. The top panel shows the cumulative modeled fraction of N_2O (above background) from each of the four categories waste, energy, direct, and indirect soil emissions, summing to 1. The second panel shows the observations (red) and 1σ error (shaded red) and the simulation without added seasonality (dark green) and with seasonality (green) in emissions. The third panel shows the residuals. The bottom left panel shows the direct comparison between simulated and observed mole fractions. A 1:1 line is shown in black, and the fits for no seasonality/seasonality simulations as dashed lines. The bottom center and right panels show the daily and monthly deviations from the overall mean for the observations and the model.

simulation; and R_i^X is the isotopic signature of source *i* estimated from the literature as described in section 2.5 and Table 1. C_b and R_b^X are the N_2O mole fraction and isotopic composition of background air, respectively (section 3.3). Delta values were calculated relating simulated isotope ratios to the international scales. The simulated source isotopic composition values for the whole experimental period are shown on the two-isotope plot (Figure 4) for comparison with the estimated ranges for different source categories (Table 1) and the measured source isotopic composition found with equation (2).

The simulation was able to capture the mean diurnal cycle in isotopic composition for $\delta^{18}O$, SP, and $\delta^{15}N^{bulk}$ (data not shown), as both the estimated source signatures and the measured sources are isotopically lighter than the background (Figure 4). However, when only results from a certain time period were considered (e.g., 15:00 and 21:00 when agreement in mole fraction between simulation and observations was best), there was no agreement between simulated and measured isotopic composition. Similarly, there was no correlation between monthly mean simulated and measured values. To investigate only the effect of partitioning between different source types, the isotopic composition was also simulated using the modeled fractions of different sources together with the measured total N_2O mole fraction above background. This did not improve agreement between simulated and measured isotopic composition, which still only showed correlation due to the average diurnal cycle.

The mean simulated source isotopic compositions are significantly different from the mean measured values for all three isotopocules (Figure 4). The difference is particularly striking for $\delta^{15}N^{bulk}$, where almost all measured source isotopic composition fall above the mean simulated source isotopic composition. In addition, the measured source isotopic compositions show up to 20 times greater variability than the simulated source isotopic compositions, as shown in the scatter of the two data sets in Figure 4. The poor capability of the model to simulate isotopic composition at Dübendorf is likely due to uncertainties in both the modeled fractions of N_2O from each source at the site and the estimated isotopic signatures for different sources types (Table 1). The range of measured source isotopic composition is even larger than the total range of literature-estimated source signatures. This is a strong indication that the true range of source isotopic signatures is likely to be larger than estimated from the literature, particularly for SP. The lack of representative literature values for source isotopic signatures appears to be the major limitation on the use of N_2O isotopic data to refine emission estimates with inverse models; the small signal to noise ratio for N_2O mole fraction and isotopic composition data will also be challenging for emission estimates on the regional scale.

4. Discussion

N_2O isotopic composition was measured at Dübendorf for 19 months, between July 2014 and February 2016, to produce the first long-term semicontinuous data set with high time resolution ($<1\ h^{-1}$ during intensive measurement periods) at a suburban site. Total source isotopic composition was determined for 1 and 5 day moving windows and compared to online measurements of chemical and meteorological parameters. Additionally, N_2O mole fraction and isotopic composition were modeled using FLEXPART-COSMO transport simulations, EDGAR inventory emissions, and literature estimates of isotopic signatures for different source categories.

To improve simulated N_2O mole fraction, seasonality was added to several of nonagricultural source categories within the EDGAR inventory; these categories represented ~15% of the total above background N_2O at Dübendorf, and the resulting seasonality of the total emissions was <5%. Simulations using emissions modified with seasonality agreed better with the observed data than simulations with unmodified EDGAR emissions. The model was able to capture the significant seasonality in observed N_2O mole fraction, whereby higher above background N_2O mole fractions were seen in winter due primarily to meteorology, even though 85% of emissions did not have seasonal variability. This suggests that N_2O emissions from the remaining sources (primarily soils and wastewater treatment) do not show strong seasonality in Switzerland. In contrast, *Thompson et al.* [2011] found significant seasonality in total N_2O emissions in many European regions using an inversion approach. Our study site is particularly responsive to local-regional scale emissions, and our results suggest that the temporal variability of N_2O emissions shows high spatial and/or interannual variability—as large in magnitude as possible seasonal cycles—in agreement with global model results from *Saikawa et al.* [2013]. The major N_2O sources at Dübendorf are expected to be soil and agriculture [*FOEN*, 2016] (Figures 1 and 8). N_2O emissions from these sources have been shown to vary in response to many factors, such as animal

stocks, fertilizer application, crop types, and tillage [*Buckingham et al.*, 2014; *Ruser et al.*, 2006; *Six et al.*, 2002; *Smith et al.*, 1998], as well as climate and soil parameters [*McDaniel et al.*, 2014; *Stehfest and Bouwman*, 2006; *Papen and Butterbach-Bahl*, 1999; *Bouwman*, 1996]. Thus, it appears that temporal variability in N_2O emissions from soils and agricultural sources cannot be parameterized by a simple seasonality function but may require a more complex process-based model [*Kraus et al.*, 2014; *Butterbach-Bahl et al.*, 2001].

Considering correlations with various pollution tracers as well as the source region of air reaching the Dübendorf site, the factors affecting measured N_2O source isotopic composition were considered. $\delta^{18}O$ shows a strong, consistent relationship to pollution index (Figure 5; correlation significant at $p < 0.01$); therefore, it is clearly the best isotopic tracer of urban/industry-emitted N_2O in Dübendorf. This is consistent with measurements from the urban area of Boston, which showed much higher variability in $\delta^{18}O$ than in SP and $\delta^{15}N^{bulk}$ [*Harris et al.*, 2014]. Our results were able to distinguish between clean air influence with low $\delta^{18}O$ and high $\delta^{15}N^{bulk}$ and a local or southwest influenced, more polluted regime with high $\delta^{18}O$ and low $\delta^{15}N^{bulk}$. In contrast to the trend over the majority of the measurements, air from the northeastern sector resulted in source signatures with low $\delta^{18}O$ and very high $\delta^{15}N^{bulk}$ despite moderately high pollution index (cluster 4, Figure 7). Seasonality in measured source isotopic composition is much higher for urban/industrially polluted transport regimes, and source isotopic composition is higher in summer than winter. Low $\delta^{18}O$ and high $\delta^{15}N^{bulk}$ can be associated with agricultural and natural soil-derived N_2O, based on correlations with tracers and transport—in contrast to literature estimates of source isotopic signatures, which generally show lower $\delta^{15}N^{bulk}$ for soil-derived N_2O (Figure 4 and Table 1). Thus, cleaner air measured at Dübendorf (i.e., less industrial/urban pollution) has a greater proportion of soil-derived N_2O, while air from the local area and the southwest region has more N_2O emitted by nonsoil sources, such as energy and industry. Northeast transport results in urban/industry-influenced air at the site, based on pollution tracers, but N_2O which is isotopically consistent with agriculture. This could be explained by low combustion efficiency in this region, resulting in elevated pollution index, thus illustrating the advantages of the isotopic approach to distinguish source classes compared to tracer-tracer and other approaches.

The variability in measured isotopic composition of the total source (Figures 3 and 4) was much larger than the simulated source isotopic composition, which uses literature estimates of isotopic signatures for the different source categories combined with FLEXPART-COSMO transport modeling. The measured $\delta^{18}O$ and SP values for the total source were relatively similar to the prior estimates; however, almost all measured values for $\delta^{15}N^{bulk}$ were higher than the estimated signatures (Figure 4). The globally averaged anthropogenic source isotopic composition has been estimated from long-term time series in several studies to be between −6 and 36‰ for $\delta^{18}O$ and −19 and −6‰ for $\delta^{15}N^{bulk}$ [*Sowers et al.*, 2002; *Röckmann et al.*, 2003; *Ishijima et al.*, 2007; *Toyoda et al.*, 2013]; results for SP are inconclusive. We calculate a mean anthropogenic source isotopic composition of 25.4 ± 9.6‰, -0.3 ± 6.4‰, and 9.2 ± 8.3‰ for $\delta^{18}O$, $\delta^{15}N^{bulk}$, and SP, respectively. Our measured value for the total source $\delta^{18}O$ falls well within the range for global studies; however, $\delta^{15}N^{bulk}$ is higher than global values.

We conclude that the variability of isotopic composition within different source types is extremely high, particularly for $\delta^{15}N^{bulk}$ and SP—similar to the differences between source types. Seasonality is complex: Isotopic composition is higher for all isotopologues in winter than in summer ($p < 0.01$), which cannot be explained by seasonally varying proportions of different source processes, as $\delta^{15}N^{bulk}$ is decoupled from $\delta^{18}O$ and SP spatially and across source types. For example, if seasonal variability in the magnitude of the soil source caused the seasonal cycle in isotopic composition, we would expect $\delta^{15}N^{bulk}$ to be higher in summer and SP to have the smallest magnitude in seasonal cycle. The consistency in the seasonal cycle for all three delta values may therefore suggests that reduction of N_2O by denitrifiers has a much greater influence in winter, causing N_2O from soils to have enriched isotopic composition, particularly evident in cluster 4 (NE) results (Figure 7). In contrast to the measurements, the variability in simulated source isotopic signature is very low—1–2 orders of magnitude less than measured (Figure 4)—suggesting that the signatures in isotopic composition from literature strongly underestimate the true variability in source isotopic composition.

Isotopic signatures have been used as "fingerprints" for different microbial processes or for the imprint of agricultural and total anthropogenic N_2O on the preindustrial background [*Perez et al.*, 2001; *Röckmann et al.*, 2003; *Toyoda et al.*, 2011; *Park et al.*, 2011; *Well et al.*, 2012]. Similarly to CH_4, it has been suggested that interpretation of N_2O isotopic composition could be extended to distinguish between different anthropogenic source classes [*Lowe et al.*, 1994; *Conny and Currie*, 1996; *Rigby et al.*, 2012; *Röckmann et al.*, 2016]. However, the

results of this study suggest that for $\delta^{15}N^{bulk}$ and SP the variability within N_2O source classes, due to responses to many climatological, natural, and agricultural parameters, is as large as the differences between classes. $\delta^{15}N^{bulk}$ and SP of N_2O are likely to provide more insight into the microbial and chemical processes leading to emission than the emission category, while $\delta^{18}O$ may be a useful indicator of industrial/urban versus soil N_2O emissions.

5. Conclusions

Preconcentration coupled with quantum cascade laser spectroscopy offers the potential for semicontinuous, online measurements of N_2O isotopic composition with long-term stability and precision comparable to traditional IRMS measurements. Analysis of a 19 month time series from Dübendorf, Switzerland, revealed that $\delta^{18}O$ is the best isotopic indicator of industrial/urban versus agricultural N_2O, while SP and $\delta^{15}N^{bulk}$ show no consistent dependence on specific sources. Comparison to model simulations showed that literature estimates of source isotopic signatures strongly underestimate the true variability of these values, and a large number of additional direct measurements of source isotopic composition are needed before ambient N_2O isotopic composition can be successfully applied to inversely infer emission strengths by source type on the regional scale.

Isotopic measurements of N_2O are particularly challenging to interpret on a regional scale with a complex mixture of sources. At the site scale, where only a small number of well-defined sources dominate—for example, microbial N_2O production from agriculture—isotopic measurements can be used to understand variability in N_2O production pathways. Similarly, on the global scale over longer time periods, isotopic composition will reflect decadal changes in the mean anthropogenic source and improve our understanding of changing anthropogenic N_2O emissions. Between the site and global scales, significant further investigations are needed, in particular, regarding a thorough knowledge of the factors affecting source isotopic signatures. In combination with the development of complex process and transport models for N_2O emissions, online analysis of N_2O isotopic composition with P-QCLAS could offer significant potential to improve our understanding of the N_2O budget.

Acknowledgments
The authors would like to thank Naohiro Yoshida and Sakae Toyoda from the Tokyo Institute of Technology for assistance with calibration and intercomparison. We also thank MeteoSwiss for access to their operational COSMO analysis products and the Swiss National Supercomputing Centre (CSCS) where FLEXPART-COSMO simulations were performed. Instrumental developments at Empa were funded by the European Metrology Research Programme (EMRP)ENV52 project "Metrology for high-impact greenhouse gases." The EMRP is jointly funded by the EMRP participating countries within EURAMET and the European Union. Eliza Harris was supported by the European Union's Seventh Framework Programme for research, technological development, and demonstration under grant agreement 2010e267161, and by the SNSF under grant 200021L_150237 and supplementary grant 200021L_150237/2. All data cited in this paper are available through PANGAEA: Data Publisher for Earth & Environmental Science according to the AGU Data Policy at https://doi.pangaea.de/10.1594/PANGAEA.864305.

References

Amon, B., V. Kryvoruchko, T. Amon, and S. Zechmeister-Boltenstern (2006), Methane, nitrous oxide and ammonia emissions during storage and after application of dairy cattle slurry and influence of slurry treatment, *Agric. Ecosyst. Environ.*, *112*, 153–162, doi:doi:10.1016/j.agee.2005.08.030. [Available at http://linkinghub.elsevier.com/ retrieve/pii/S0167880905004135.]

Baldauf, M., A. Seifert, J. Förstner, D. Majewski, M. Raschendorfer, and T. Reinhardt (2011), Operational convective-scale numerical weather prediction with the COSMO model: Description and sensitivities, *Mon. Weather Rev.*, *139*, 3887–3905, doi:10.1175/MWR-D-10-05013.1.

Bergamaschi, P., et al. (2015), Top-down estimates of European CH_4 and N_2O emissions based on four different inverse models, *Atmos. Chem. Phys.*, *15*, 715–736, doi:10.5194/acp-15-715-2015.

Bouwman, A. F. (1996), Direct emission of nitrous oxide from agricultural soils, *Nutrient Cycling Agroecosyst.*, *46*, 53–70, doi:10.1007/BF00210224. [Available athttp://link.springer.com/10.1007/BF00210224.]

Bouwman, A. F., K. W. V. D. Hoek, and J. G. J. Olivier (1995), Uncertainties in the global source distribution of nitrous oxide, *J. Geophys. Res.*, *100*, 2785–2800.

Buckingham, S., S. Anthony, P. H. Bellamy, L. M. Cardenas, S. Higgins, K. McGeough, and C. F. E. Topp (2014), Review and analysis of global agricultural NO emissions relevant to the UK, *Sci. Total Environ.*, *487*, 164–172, doi:10.1016/j.scitotenv.2014.02.122. [Available at http://www.ncbi.nlm.nih.gov/pubmed/24784741.]

Bühlmann, T., B. Achermann, S. Liechti, B. R. Locher, R. Hiltbrunner, and C. Koerner (2014), Durch Stickstoffdeposition induzierte Emissionen von Stickoxiden und Lachgas aus (semi-) natürlichen Ökosystemen, *Tech. Rep.*, BAFU, Abteilung Luftreinhaltung und Chemikalien, Bern, Switzerland.

Bühlmann, T., E. Hiltbrunner, C. Körner, B. Rihm, and B. Achermann (2015), Induction of indirect N_2O and NO emissions by atmospheric nitrogen deposition in (semi-)natural ecosystems in Switzerland, *Atmos. Environ.*, *103*, 94–101, doi:10.1016/j.atmosenv.2014.12.037. [Available at http://linkinghub.elsevier.com/retrieve/pii/ S1352231014009856.]

Butterbach-Bahl, K., F. Stange, H. Papen, and C. Li (2001), Regional inventory of nitric oxide and nitrous oxide emissions for forest soils of southeast Germany using the biogeochemical model PnET-N-DNDC, *J. Geophys. Res.*, *106*, 34,155–34,166, doi:10.1029/2001JD000173.

Carter, M. S., et al. (2012), Synthesizing greenhouse gas fluxes across nine European peatlands and shrublands—Responses to climatic and environmental changes, *Biogeosciences*, *9*, 3739–3755, doi:10.5194/bg-9-3739-2012. [Available at http://www.biogeosciences.net/9/3739/2012/.]

Conny, J. M., and L. A. Currie (1996), The isotopic characterization of methane, non-methane hydrocarbons and formaldehyde in the troposphere, *Atmos. Environ.*, *30*, 621–638, doi:10.1016/1352-2310(95)00305-3.

Eyer, S., et al. (2016), Real-time analysis of $\delta^{13}C$- and δD-CH_4 in ambient methane with laser spectroscopy: Method development and first inter-comparison results, *Atmos. Meas. Tech.*, *9*, 263–280, doi:10.5194/amt-9-263-2016.

Federal Office for the Environment (FOEN) (2016), Switzerland's greenhouse gas inventory, 1990–2014, *Tech. Rep.*, Bern, Switz.

Harris, E., D. D. Nelson, W. Olszewski, M. Zahniser, K. E. Potter, B. J. McManus, A. Whitehill, R. G. Prinn, and S. Ono (2014), Development of a spectroscopic technique for continuous online monitoring of oxygen and site-specific nitrogen isotopic composition of atmospheric nitrous oxide, *Anal. Chem.*, *86*, 1726–1734, doi:10.1021/ac403606u.

Harris, E., A. Joss, L. Emmenegger, M. Kipf, B. Wolf, J. Mohn, and P. Wunderlin (2015a), Isotopic evidence for nitrous oxide production pathways in a partial nitritation-anammox reactor, *Water Res.*, *83*, 258–270, doi:10.1016/j.watres.2015.06.040.

Harris, E., K. Zeyer, R. Kegel, B. Müller, L. Emmenegger, and J. Mohn (2015b), Nitrous oxide and methane emissions and nitrous oxide isotopic composition from waste incineration in Switzerland, *Waste Manage.*, *35*, 135–140, doi:10.1016/j.wasman.2014.10.016.

Heil, J., B. Wolf, N. Brueggemann, L. Emmenegger, B. Tuzson, H. Vereecken, and J. Mohn (2014), Site-specific ^{15}N signatures of abiotically-produced N2O, *Geochim. Cosmochim. Acta*, *139*, 72–82, doi:10.1016/j.gca.2014.04.037.

Henne, S., D. Brunner, B. Oney, M. Leuenberger, W. Eugster, I. Bamberger, F. Meinhardt, M. Steinbacher, and L. Emmenegger (2016), Validation of the Swiss methane emission inventory by atmospheric observations and inverse modelling, *Atmos. Chem. Phys.*, *16*, 3683–3710.

Hotz, M.-C., and F. Weibel (2005), Arealstatistik Schweiz: Zahlen - Fakten-Analysen, *Tech. Rep.*, Neuchatel, Switzerland.

Intergovernmental Panel on Climate Change (IPCC) (2013), *Climate Change 2013: The Physical Science Basis—Working Group 1 Contribution to the Fifth Assessment Report of the Intergovernmental Panel on Climate Change*, Cambridge Univ. Press, Cambridge, U. K.

Ishijima, K., S. Sugawara, K. Kawamura, G. Hashida, S. Morimoto, S. Murayama, S. Aoki, and T. Nakazawa (2007), Temporal variations of the atmospheric nitrous oxide concentration and its delta N-15 and delta O-18 for the latter half of the 20th century reconstructed from firn air analyses, *J. Geophys. Res.*, *112*, D03305, doi:10.1029/2006JD007208.

JRC/PBL (2009), Emission Database for Global Atmospheric Research (EDGAR), release version 4.0, *Tech. Rep.*, European Commission, Joint Research Centre (JRC)/Netherlands Environmental Assessment Agency (PBL) [Available at http://edgar.jrc.ec.europa.eu.]

Kaiser, J., C. A. M. Brenninkmeijer, and T. Rockmann (2002), Intramolecular N-15 and O-18 fractionation in the reaction of N_2O with O(D-1) and its implications for the stratospheric N_2O isotope signature, *J. Geophys. Res.*, *107*, 4214, doi:10.1029/2001JD001506.

Kaiser, J., A. Engel, R. Borchers, and T. Rockmann (2006), Probing stratospheric transport and chemistry with new balloon and aircraft observations of the meridional and vertical N_2O isotope distribution, *Atmos. Chem. Phys.*, *6*, 3535–3556.

Keeling, C. D. (1958), The concentration and isotopic abundances of atmospheric carbon dioxide in rural areas, *Geochim. Cosmochim. Acta*, *13*, 322–334, doi:10.1016/0016-7037(58)90033-4.

Keeling, C. D. (1960), The concentration and isotopic abundances of carbon dioxide in rural and marine air, *Tellus*, *24*, 277–298, doi:10.1016/0016-7037(61)90023-0.

Kim, K. R., and H. Craig (1993), N-15 and O-18 characteristics of nitrous-oxide—A global perspective, *Science*, *262*, 1855–1857, doi:10.1126/science.262.5141.1855.

Kraus, D., S. Weller, S. Klatt, E. Haas, R. Wassmann, R. Kiese, and K. Butterbach-Bahl (2014), A new Landscape DNDC biogeochemical module to predict CH_4 and N_2O emissions from lowland rice and upland cropping systems, *Plant Soil*, doi:10.1007/s11104-014-2255-x. [Available at http: //link.springer.com/10.1007/s11104-014-2255-x.]

Lowe, D. C., C. A. M. Brenninkmeijer, G. W. Brailsford, K. R. Lassey, A. J. Gomez, and E. G. Nisbet (1994), Concentration and ^{13}C records of atmospheric methane in New Zealand and Antarctica: Evidence for changes in methane sources, *J. Geophys. Res.*, *99*, 16,913–16,925, doi:10.1029/94JD00908. [Available at https://doi.org/10.1029/94JD00908.]

Maeda, K., S. Toyoda, R. Shimojima, T. Osada, D. Hanajima, R. Morioka, and N. Yoshida (2010), Source of nitrous oxide emissions during the cow manure composting process as revealed by isotopomer analysis of and AMOA abundance in betaproteobacterial ammonia-oxidizing bacteria, *Appl. Environ. Microbiol.*, *76*, 1555–1562, doi:10.1128/AEM.01394-09.

McDaniel, M. D., J. P. Kaye, and M. W. Kaye (2014), Do "hot moments" become hotter under climate change? Soil nitrogen dynamics from a climate manipulation experiment in a post-harvest forest, *Biogeochemistry*, *121*, 339–354, doi:10.1007/s10533-014-0001-3.

Miller, J. B., and P. P. Tans (2003), Calculating isotopic fractionation from atmospheric measurements at various scales, *Tellus B*, *55*, 207–214, doi:10.1034/j.1600-0889.2003.00020.x.

Mohn, J., C. Guggenheim, B. Tuzson, M. K. Vollmer, S. Toyoda, N. Yoshida, and L. Emmenegger (2010), A liquid nitrogen-free preconcentration unit for measurements of ambient N_2O isotopomers by QCLAS, *Atmos. Meas. Tech.*, *3*, 609–618, doi:10.5194/amt-3-609-2010.

Mohn, J., B. Tuzson, A. Manninen, N. Yoshida, S. Toyoda, W. A. Brand, and L. Emmenegger (2012), Site selective real-time measurements of atmospheric N_2O isotopomers by laser spectroscopy, *Atmos. Meas. Tech.*, *5*, 1601–1609.

Mohn, J., et al. (2014), Interlaboratory assessment of nitrous oxide isotopomer analysis by isotope ratio mass spectrometry and laser spectroscopy: Current status and perspectives, *Rapid Communications In Mass Spectrometry*, *28*, 1995–2007, doi:10.1002/rcm.6982.

NABEL (2015), Technischer Bericht zum Nationalen Beobachtungsnetz für Luftfremdstoffe (NABEL), *Tech. Rep.*, Dübendorf.

Ogawa, M., and N. Yoshida (2005a), Nitrous oxide emission from the burning of agricultural residue, *Atmos. Environ.*, *39*, 3421–3429, doi:10.1016/j.atmosenv.2005.01.059.

Ogawa, M., and N. Yoshida (2005b), Intramolecular distribution of stable nitrogen and oxygen isotopes of nitrous oxide emitted during coal combustion, *Chemosphere*, *61*, 877–87, doi:10.1016/j.chemosphere.2005.04.096. [Available at http://www.ncbi.nlm.nih.gov/pubmed/15993467.]

Olivier, J. G. J., A. F. Bouwman, C. W. M. van der Maas, and J. J. M. Berdowski (1994), Emission database for global atmospheric research (EDGAR), *Environ. Monitor. Assess.*, *31*, 93–106.

Owen, J. J., and W. L. Silver (2014), Greenhouse gas emissions from dairy manure management: A review of field-based studies, *Global Change Biol.*, doi:10.1111/gcb.12687. [Available at http://www.ncbi.nlm.nih.gov/pubmed/ 25044806.]

Pandey Deolal, S., S. Henne, L. Ries, S. Gilge, U. Weers, M. Steinbacher, J. Staehelin, and T. Peter (2014), Analysis of elevated springtime levels of Peroxyacetyl nitrate (PAN) at the high Alpine research sites Jungfraujoch and Zugspitze, *Atmos. Chem. Phys.*, *16*, 12,553–12,571, doi:10.5194/acp-14-12553-2014.

Papen, H., and K. Butterbach-Bahl (1999), A 3-year continuous record of nitrogen trace gas fluxes spruce and beech forest ecosystem in Germany: 1. N_2O emissions, *J. Geophys. Res.*, *104*, 18,487–18,503, doi:10.1029/1999JD900293.

Park, S., T. Perez, K. A. Boering, S. E. Trumbore, J. Gil, S. Marquina, and S. C. Tyler (2011), Can N_2O stable isotopes and isotopomers be useful tools to characterize sources and microbial pathways of N_2O production and consumption in tropical soils?, *Global Biogeochem. Cycles*, *25*, GB1001, doi:10.1029/2009GB003615.

Park, S., et al. (2012), Trends and seasonal cycles in the isotopic composition of nitrous oxide since 1940, *Nat. Geosci.*, *5*, 261–265, doi:10.1038/NGEO1421.

Perez, T., S. E. Trumbore, S. C. Tyler, P. A. Matson, I. Ortiz-Monasterio, T. Rahn, and D. W. T. Griffith (2001), Identifying the agricultural imprint on the global N_2O budget using stable isotopes, *J. Geophys. Res.*, *106*, 9869–9878, doi:10.1029/2000JD900809.

Prather, M. J., et al. (2015), Measuring and modeling the lifetime of nitrous oxide including its variability, *J. Geophys. Res. Atmos.*, *120*, 5693–5705, doi:10.1002/2015JD023267.

Prinn, R. G., et al. (2000), A history of chemically and radiatively important gases in air deduced from ALE/GAGE/AGAGE, *J. Geophys. Res.*, *105*, 17,751–17,792.

Prinn, R. G., et al. (2013), *The ALE/GAGE AGAGE Network*, Carbon Dioxide Inf. Anal. Cent. (CDIAC), Oak Ridge Natl. Lab. (ORNL), U.S. Dep. of Energy (DOE).

Rahn, T., and M. Wahlen (1997), Stable isotope enrichment in stratospheric nitrous oxide, *Science*, *278*, 1776–1778, doi:10.1126/science.278.5344.1776. [Available at http://www.sciencemag.org/cgi/doi/10.1126/science.278. 5344.1776.]

Rapson, T. D., and H. Dacres (2014), Analytical techniques for measuring nitrous oxide, *Trends Anal. Chem.*, *54*, 65–74, doi:10.1016/j.trac.2013.11.004. [Available at https://doi.org/10.1016/j.trac.2013.11.004.]

Ravishankara, A. R., J. S. Daniel, and R. W. Portmann (2009), Nitrous oxide (N_2O): The dominant ozone-depleting substance emitted in the 21st century, *Science*, *326*, 123–125, doi:10.1126/science.1176985.

Rigby, M., A. J. Manning, and R. G. Prinn (2012), The value of high-frequency, high-precision methane isotopologue measurements for source and sink estimation, *J. Geophys. Res.*, *117*, D12312, doi:10.1029/2011JD017384.

Röckmann, T., J. Kaiser, and C. A. M. Brenninkmeijer (2003), The isotopic fingerprint of the pre-industrial and the anthropogenic N_2O source, *Atmos. Chem. Phys.*, *3*, 315–323.

Röckmann, T., et al. (2016), In-situ observations of the isotopic composition of methane at the Cabauw tall tower site, *Atmos. Chem. Phys. Discuss.*, *16*(16), 10,469–10,487, doi:10.5194/acp-16-10469-2016.

Ruser, R., H. Flessa, R. Russow, G. Schmidt, F. Buegger, and J. Munch (2006), Emission of N_2O, N_2 and CO_2 from soil fertilized with nitrate: Effect of compaction, soil moisture and rewetting, *Soil Biol. Biochem.*, *38*, 263–274, doi:10.1016/j.soilbio.2005.05.005. [Available at http://linkinghub.elsevier.com/retrieve/pii/S0038071705001975.]

Saikawa, E., C. A. Schlosser, and R. G. Prinn (2013), Global modeling of soil nitrous oxide emissions from natural processes, *Global Biogeochem. Cycles*, *27*, 972–989, doi:10.1002/gbc.20087. [Available at http://doi.wiley.com/10.1002/gbc.20087.]

Seibert, P., and A. Frank (2004), Source-receptor matrix calculation with a Lagrangian particle dispersion model in backward mode, *Atmos. Chem. Phys.*, *4*, 51–63, doi:10.5194/acp-4-51-2004. [Available at http: //www.atmos-chem-phys.net/4/51/2004/.]

Six, J., C. Feller, K. Denef, S. M. Ogle, J. C. de Moraes Sa, and A. Albrecht (2002), Soil organic matter, biota and aggregation in temperate and tropical soils—Effects of no-tillage, in *International Nitrogen Workshop*, vol. 22, pp. 755–775, Agronomie, Reims, France.

Smith, K., P. Thomson, H. Clayton, I. Mctaggart, and F. Conen (1998), Effects of temperature, water content and nitrogen fertilisation on emissions of nitrous oxide by soils, *Atmos. Environ.*, *32*, 3301–3309, doi:10.1016/S1352-2310(97)00492-5. [Available at http://linkinghub.elsevier.com/retrieve/pii/S1352231097004925.]

Snider, D., K. Thompson, C. Wagner-Riddle, J. Spoelstra, and K. Dunfield (2015), Molecular techniques and stable isotope ratios at natural abundance give complementary inferences about N_2O production pathways in an agricultural soil following a rainfall event, *Soil Biol. Biochem.*, *88*, 197–213, doi:10.1016/j.soilbio.2015.05.021. [Available at http://linkinghub.elsevier.com/retrieve/pii/S0038071715001911.]

Snover, A. K., P. D. Quay, and W. M. Hao (2000), The D/H content of methane emitted from biomass burning, *Global Biogeochem. Cycles*, *14*, 11–24, doi:10.1029/1999GB900075.

Sowers, T., A. Rodebaugh, N. Yoshida, and S. Toyoda (2002), Extending records of the isotopic composition of atmospheric N_2O back to 1800 A.D. from air trapped in snow at the South Pole and the Greenland Ice Sheet Project II ice core, *Global Biogeochem. Cycles*, *16*, 1129, doi:10.1029/2002GB001911.

Stehfest, E., and L. Bouwman (2006), N_2O and NO emission from agricultural fields and soils under natural vegetation: summarizing available measurement data and modeling of global annual emissions, *Nutrient Cycling Agroecosyst.*, *74*, 207–228, doi:10.1007/s10705-006-9000-7. [Available at http://link.springer.com/10.1007/ s10705-006-9000-7.]

Stohl, A., C. Forster, A. Frank, P. Seibert, and G. Wotawa (2005), Technical note: The Lagrangian particle dispersion model FLEXPART version 6.2, *Atmos. Chem. Phys.*, *5*, 2461–2474.

Sutka, R. L., N. E. Ostrom, P. H. Ostrom, J. A. Breznak, H. Gandhi, A. J. Pitt, and F. Li (2006), Distinguishing nitrous oxide production from nitrification and denitrification on the basis of isotopomer abundances, *Appl. Environ. Microbiol.*, *72*, 638–644, doi:10.1128/AEM.72.1.638-644.2006.

Thiemens, M. H., and W. C. Trogler (1991), Nylon production—An unknown source of atmospheric nitrous oxide, *Science*, *251*, 932–934, doi:10.1126/science.251.4996.932.

Thompson, R. L., C. Gerbig, and C. Rödenbeck (2011), A Bayesian inversion estimate of N_2O emissions for western and central Europe and the assessment of aggregation errors, *Atmos. Chem. Phys.*, *11*, 3443–3458, doi:10.5194/acp-11-3443-2011.

Thompson, R. L., et al. (2014a), Nitrous oxide emissions 1999 to 2009 from a global atmospheric inversion, *Atmos. Chem. Phys.*, *14*, 1801–1817, doi:10.5194/acp-14-1801-2014.

Thompson, R. L., et al. (2014b), TransCom N_2O model inter-comparison—Part 2: Atmospheric inversion estimates of N_2O emissions, *Atmos. Chem. Phys.*, *14*, 6177–6194, doi:10.5194/acp-14-6177-2014.

Toyoda, S., and N. Yoshida (1999), Determination of nitrogen isotopomers of nitrous oxide on a modified isotope ratio mass spectrometer, *Anal. Chem.*, *71*, 4711–4718, doi:10.1021/ac9904563.

Toyoda, S., et al. (2004), Temporal and latitudinal distributions of stratospheric N_2O isotopomers, *J. Geophys. Res.*, *109*, D08308, doi:10.1029/2003JD004316.

Toyoda, S., S.-i. Yamamoto, S. Arai, H. Nara, N. Yoshida, K. Kashiwakura, and K.-I. Akiyama (2008), Isotopomeric characterization of N_2O produced, consumed, and emitted by automobiles, *Rapid Commun. Mass Spectrom.*, *22*, 603–612, doi:10.1002/rcm.3400.

Toyoda, S., Y. Suzuki, S. Hattori, K. Yamada, A. Fujii, N. Yoshida, R. Kouno, K. Murayama, and H. Shiomi (2011), Isotopomer analysis of production and consumption mechanisms of N_2O and CH_4 in an advanced wastewater treatment system, *Environ. Sci. Technol.*, *45*, 917–922, doi:10.1021/es102985u.

Toyoda, S., N. Kuroki, N. Yoshida, K. Ishijima, Y. Tohjima, and T. Machida (2013), Decadal time series of tropospheric abundance of N_2O isotopomers and isotopologues in the Northern Hemisphere obtained by the long-term observation at Hateruma Island, Japan, *J. Geophys. Res. Atmos.*, *118*, 3369–3381, doi:10.1002/jgrd.50221.

Vardag, S. N., S. Hammer, and I. Levin (2016), Evaluation of 4 years of continuous $\delta^{13}C(CO_2)$ data using a moving Keeling plot method, *Biogeosciences*, *13*, 4237–4251, doi:10.5194/bg-13-4237-2016.

Vitousek, P. M., D. N. L. Menge, S. C. Reed, and C. C. Cleveland (2013), Biological nitrogen fixation: Rates, patterns and ecological controls in terrestrial ecosystems, *Philos. Trans. R. Soc. B*, *368*(20130119), doi:10.1098/rstb.2013.0119. [Available at http://www.ncbi.nlm.nih.gov/pubmed/23713117.]

Wanner, H., and M. Furger (1990), The Bise—Climatology of a regional wind north of the Alps, *Meteorol. Atmos. Phys.*, *43*, 105–115, doi:10.1007/BF01028113.

Well, R., W. Eschenbach, H. Flessa, C. von der Heide, and D. Weymann (2012), Are dual isotope and isotopomer ratios of N_2O useful indicators for N_2O turnover during denitrification in nitrate-contaminated aquifers?, *Geochim. Cosmochim. Acta*, *90*, 265–282, doi:10.1016/j.gca.2012.04.045.

Werner, R. A., and W. A. Brand (2001), Referencing strategies and techniques in stable isotope ratio analysis, *Rapid Commun. Mass Spectrom.*, *15*, 501–519, doi:10.1002/rcm.258.

Whiticar, M., and H. Schaefer (2007), Constraining past global tropospheric methane budgets with carbon and hydrogen isotope ratios in ice, *Philos. Trans. A*, *365*, 1793–1828, doi:10.1098/rsta.2007.2048.

Wolf, B., X. Zheng, N. Brüggemann, W. Chen, M. Dannenmann, X. Han, M. A. Sutton, H. Wu, Z. Yao, and K. Butterbach-Bahl (2010), Grazing-induced reduction of natural nitrous oxide release from continental steppe, *Nature*, *464*, 881–444, doi:10.1038/nature08931. [Available http://www.ncbi.nlm.nih.gov/pubmed/20376147.]

Wolf, B., L. Merbold, C. Decock, B. Tuzson, E. Harris, J. Six, L. Emmenegger, and J. Mohn (2015), First on-line isotopic characterization of N_2O emitted from intensively managed grassland, *Biogeosciences*, *12*, 2517–2531, doi:10.5194/bg-12-2517-2015.

Wunderlin, P., J. Mohn, A. Joss, L. Emmenegger, and H. Siegrist (2012), Mechanisms of N_2O production in biological wastewater treatment under nitrifying and denitrifying conditions, *Water Res.*, *46*, 1027–1037, doi:10.1016/j.watres.2011.11.080. [Available at http://www.ncbi.nlm.nih.gov/pubmed/22227243.]